# FHBS CALCULATION OF IONIZED ELECTRON ANGULAR AND ENERGY DISTRIBUTION FOLLOWING THE $P+H$ COLLISION AT 20 $KEV$

A Dissertation

by

JUN FU

Submitted to the Office of Graduate Studies of
Texas A&M University
in partial fulfillment of the requirements for the degree of

DOCTOR OF PHILOSOPHY

August 2004

Major Subject: Physics

FHBS CALCULATION OF IONIZED ELECTRON ANGULAR AND ENERGY

DISTRIBUTION FOLLOWING THE $P+H$ COLLISION AT 20 $KEV$

A Dissertation

by

JUN FU

Submitted to Texas A&M University
in partial fulfillment of the requirements
for the degree of

DOCTOR OF PHILOSOPHY

Approved as to style and content by:

John F. Reading
(Chair of Committee)

Edward S. Fry
(Member)

David A. Church
(Member)

Rand L. Watson
(Member)

Edward S. Fry
(Head of Department)

August 2004

Major Subject: Physics

# ABSTRACT

FHBS Calculation of Ionized Electron Angular and Energy

Distribution Following the $p+H$ collision at 20 $keV$. (August 2004)

Jun Fu, B. S., Nankai University;

M.S., Texas A&M University

Chair of Advisory Committee: Dr. John F. Reading

A Finite Hilbert Basis Set (FHBS) method to calculate the angular and energy distribution of ejected electrons in an ion-atom collision is presented. This method has been applied to the $p+H$ collision at 20 $keV$ impact energy. An interference effect between the exit channels, where electrons are guided out of the collision region by both the residual target proton and the projectile proton, is discovered. Experimental data appears to confirm this result.

To Fengyu Song

# ACKNOWLEDGMENTS

The author gratefully acknowledges the guidance of his advisor, Dr. John F. Reading, throughout his years of graduate study and research. His knowledge and encouragement have been greatly appreciated. His help and suggestions on the dissertation improved its quality. It has been a pleasure to collaborate in research and to learn physics from him.

I thank Dr. Mathew Fitzpatrick for sharing his knowledge and skills on the FHBS theory. His careful explanation of the FHBS computer program greatly helped this dissertation study.

Thanks to the physics department of Texas A&M University for the financial support. Thanks to the secretaries at the physics department for all the help I received throughout my years of graduate study.

TABLE OF CONTENTS

Page

# LIST OF TABLES

# LIST OF FIGURES

# CHAPTER I

# INTRODUCTION

This dissertation presents a *Finite Hilbert Basis Set* (FHBS) method to calculate the energy and angular distribution of ejected electrons in an ion-atom collision. This method has been applied to the $p+H$ system at 20 keV projectile energy. An unexpected interference effect has been discovered. There is an important interference in the exit channel where electrons are guided out of the collision region by both the residual target proton and the projectile proton. Experimental data appears to confirm this result.

## A. Background

This work is part of a continuing effort trying to theoretically re-produce differential cross sections in the ion-atom collision. In [1] Penhoat *el al* have noted the need for $K-$ and $L$-shell electron ionization cross sections in the fast ion-atom interaction in a living cell. They seek a better understanding of the cell death process in an ion-therapy. During this process, a fast moving ion would ionize one electron from a DNA chain, producing a K-shell vacancy. The subsequent Auger electron could then cause a break in the second chain at an adjacent site. This *double stand break* results in cell death. But the situation is complicated by the original ionized electron which also deposits energy in the cell. What is needed for a thorough investigation is a good theoretical description of the energy and angular distribution of the ionized electrons.

In answer to this challenge, we set out to use a FHBS method in a Hartree-Fock model to simulate the ion and many-electron atom collision. We start with applying our method to the $p+H$ collision, where there is only one electron. By choosing a simple system it

---

The journal model is Physical Review Letters.

is easier to check the validity of our theoretical model and calculation. Experimental data for $p+H$ collision is available [2] [3], as well as calculations from several other theories. By comparing our calculation with these data we gain experience in obtaining differential cross sections and a better understanding of the collision process.

In the $p+H$ collision we are studying, the initial target electron is in the $1s$ ground state. There are three possibilities of the electron final state after collision. This electron might still be attached to the target, either in the original ground state or in an excited higher energy bound state. It might be captured by the projectile proton, a process referred to as charge transfer. Lastly the electron might be scattered into a positive energy state. The third possibility, direct ionization, is our primary interest and is the focus of this dissertation.

In an FHBS theory there are three methods used to simulate an ion-atom collision process. The three methods differ in increasing complexity as described below.

The simplest FHBS method is the *Single-Centered Expansion* (SCE). In the SCE method a basis is confined around the target center. This limited basis has proved to be less effective in calculating charge transfer, which is important at the impact energy range we are considering (20 keV). Thus the SCE is not a good candidate to obtain meaningful differential cross sections. Despite this deficiency the SCE is helpful in checking our ability to describe the electron continuum.

The *One-and-Half-Centered-Expansion* (OHCE) method makes an improvement over the SCE method by including *bound* states on the projectile center. This enables us to effectively calculate charge transfer of electrons between the target and projectile. Previous work showed that we were able to reproduce the ejected electron energy distribution at $48keV$ projectile energy for the $p+H$ collision by using the OHCE method [4]. However, when we tried to apply this method at $20keV$ projectile energy the electron energy distribution result is rather poor. The failure is due to the stronger interaction between the projectile proton and the target electron at a lower impact energy. What we need is a pro-

jectile *continuum* channel to effectively simulate the electron ionization. This brought us to use the *Two-Centered Expansion* (TCE) method.

The TCE is a much better method to describe the ejected free electron being steered away by both the target and projectile proton; however it introduces new difficulties in obtaining the differential cross sections. In our previous work [4], we have a method to obtain the energy distribution in a single center. In adopting a TCE method, we had the problem of how to account for the energy distribution from both the target and projectile center. We could accomplish this by a Galilean transformation of the projectile energy distribution to the target frame, and then add up to the target energy distribution. However as the projectile is moving at velocity of $\mathbf{v_p}$, knowing the energy distribution in the projectile frame itself is not sufficient. The Galilean transformation requires the momentun information of the scattered electron. This mandates the development of a method to calculate the energy and angular distribution in each respective center as the very first step of our FHBS calculation.

Besides the FHBS theory, there are several other numerical approaches to calculate the ion-atom collision cross sections. The n-body Classical Trajectory Monte Carlo (CTMC) [5] [6] and the continuum-distorted-wave - eikonal-initial-state (CDW-EIS) [7] [8] [9] are two notable methods. Both CTMC and CDW-EIS are successful in obtaining cross sections in the high projectile energy range. However, both methods failed to re-produce the angular differential cross section at $20keV$ impact energy. Due to the nature of these two methods, (the CTMC is a classical method and CDW is an approximation), it is hard to evaluate their range of validity. Angular distribution results obtained by CTMC and CDW are compared to our FHBS OHCE calculations in Chapter III.

In this dissertation we use a full quantal approach towards the ion-atom collision problem. Our method is to solve the time-dependent Schrödinger equation in an FHBS representation.

Recently another quantal approach to calculate the same differential cross section

is under development. The main idea of this approach is to solve the time-dependent Schrödinger equation by using a so-called Fourier collocation method on a lattice [10]. In this method, the time-evolution operator is split approximately into three steps, where the wave function is being switched back and forth between coordinate space and momentum space [11]. At the time of this dissertation writing this method can not deal with an inter-nuclear distance greater than 50 au [12]. Since ionization is known to occur at a much larger distance, some work needs to be done in the convergence of inter-nuclear distance before this method can give reliable cross sections for a $p+H$ collision.

## B. Outline of Dissertation

The dissertation begins with an examination of the *first Born approximation* (B1) for the $p+H$ collision. Due to the nature of the FHBS method, the scattering continuum states are discretized in energy after projection and diagonization into our Hilbert space. We then use interpolation to obtain a smooth energy and angular distribution. The first Born approximation is of interest because it can provide an analytical solution to the ionization *form-factor*, against which we may check the accuracy of our interpolation. Since the FHBS is intrinsically a partial wave expansion method, we carefully examined the equivalent B1 partial wave and full-wave calculation. The number of partial wave channels needed to converge to the total cross section in B1 are studied at projectile energies of 20 $kev$ and 48 $keV$. These exact B1 partial wave results are then compared to the first Born result obtained by the FHBS calculation.

The general frame work of the FHBS method is discussed in chapter III. We first describe how to obtain a good basis for an FHBS calculation, followed by an overview of the SCE and the TCE method. The later part of the chapter discusses the method of how to extract the angular and energy distribution in a single center. The OHCE angular and

energy distribution results are given at the end of this chapter.

Obtaining the angular and energy distribution using the TCE FHBS method is discussed in chapter IV. The TCE FHBS theory distinguishes electrons associated with the target from those associated with the projectile. The target and projectile scattering probabilities are added incoherently. As the projectile is moving at velocity $\mathbf{v_p}$, to calculate the differential cross section in the lab frame the projectile scattering amplitude needs to be translated into the target frame. From chapter III we know how to calculate the scattering amplitudes as a function of momentum $\mathbf{k}'$ in projectile frame. This translation is accomplished by a simple Galilean transformation as $\mathbf{k} = \mathbf{k}' + \mathbf{v_p}$.

The translation of the scattering amplitudes causes a new problem: the original target frame scattering amplitude and translated projectile frame scattering amplitude describe electrons with the same momentum $\mathbf{k}$. These electrons are no longer distinguishable. The two amplitudes thus interfere with each other. If we are to consider interference between these two amplitudes, it is essential to calculate the phase in the wave function accurately. In FHBS method, a continuum wave function $|\chi(\varepsilon_\lambda) >$, is approximated by a basis state as $\mathbf{P}|\chi(\varepsilon_\lambda) >= N_\lambda |\chi_\lambda >$. The scattering amplitude is related to the $U$ matrix element as $T = N_\lambda U$, where $U$ is calculated using the basis state $|\chi_\lambda >$. The phase information of the wave function is preserved in $N_\lambda$. We start this chapter with the method of calculating $N_\lambda$, followed by the Galilean transformation of the projectile scattering amplitude. This transformed amplitude is then added both incoherently and coherently to the target amplitude to obtain a full angular and energy distribution for the TCE method. The results for angular and energy distribution are presented and compared with experimental data and other theoretical results at the end of this chapter.

Conclusions are drawn in chapter V.

## C. Units

Atomic Units (a.u.) are used throughout this dissertation unless otherwise noted. The atomic units are obtained by setting the following base units to unity: mass of the electron ($m_e$), Plank's constant divided by $2\pi$ representing angular momentum ($\hbar$), elementary charge ($e$), and $4\pi$ times the vacuum permittivity ($4\pi\varepsilon_0$).

Other units can be derived from these base units. Table I lists some units frequently used in this dissertation for atom with unit charge (hydrogen).

Table I. Atomic Units

| unit name | in base units | value | in a.u. |
|---|---|---|---|
| Born Radius | $a_0 = \frac{(4\pi\varepsilon_0)\hbar^2}{\mu e^2}$ | 0.529 177Å | 1 |
| 1s electron speed | $v_0 = \frac{e^2}{(4\pi\varepsilon_0)\hbar} = \alpha c$ | $2.187691 \times 10^6 \frac{m}{s}$ | 1 |
| unit energy | $E_0 = \frac{e^2}{(4\pi\varepsilon_0)\hbar}$ | 27.2114 eV | 1 |
| $1s$ energy | $\frac{E_0}{2}$ | 13.6057 eV | 0.5 |

For a K-shell atom with nucleus charge $Z$, the length and speed units are given by $a_K = a_0/Z$ and $v_K = v_0/Z$ respectively. The energy is given by

$$E_{K,n} = -\frac{Z^2}{2n^2}E_0. \tag{1.1}$$

## D. Notation

In this dissertation boldface fonts letters represent vectors. For example, $\mathbf{r}$ is used to represent a displacement in space while $\mathbf{k}$ for the momentum of an electron. Scalars are in italic, such as $r$ for the distance and $v$ for the speed of an electron. Unit vectors are in bold letter with a hat, such as $\hat{\mathbf{r}}$ is a unit vector in the $\mathbf{r}$ direction. $\mathbf{R}$ is used to describe the trajectory

of the projectile. Sometimes $\mathbf{R}$ is split into two components as $\mathbf{R}(t) = \mathbf{B} + \mathbf{v_p}t$, where $\mathbf{B}$ is the impact parameter and $\mathbf{v_p}$ is the projectile velocity.

$|\mathbf{k}>$ is used to represent an electron state with momentum $\mathbf{k}$, and $\psi(\mathbf{r})$ is used to represent a wave function in coordinate $\mathbf{r}$. For the radial part of a wave function, symbols like $\chi(r)$ are used.

Other notations will be mentioned in the text.

# CHAPTER II

## FIRST BORN CALCULATION OF THE ANGULAR DISTRIBUTION

The primary purpose of this chapter is to design a benchmark to check the validity of the FHBS method of calculating the ion-atom collision differential cross sections. The method is fully described in the next chapter. In summary: in an FHBS calculation the continuum states are discretized in energy after projection and diagonization in a chosen Hilbert space. Transition probabilities from the ground state to the continuum are calculated by using those discretized basis states. An actual continuum state wave function $|\chi(\varepsilon_\lambda)>$ is approximated by a discretized basis state, $|\chi_\lambda>$, as $\mathbf{P}|\chi(\varepsilon_\lambda)>=N_\lambda|\chi_\lambda>$. Here $\mathbf{P}$ is a projection operator. We then use interpolation method to obtain a continuous and smooth cross section to the continuum. One way to check the above approximation and interpolation methods is to compare an FHBS calculation with another independent calculation.

The first Born (B1) approximation is chosen as our benchmark because B1 is an analytical method for a $p+H$ collision. That is, for this collision the B1 approximation has an analytical expression for the *form factor*, which is then used to obtain differential cross sections. For a real $p+H$ system the $B1$ approximation treats the projectile-electron interaction as a first order perturbation. At high impact projectile velocities the B1 approximation is a good method to describe a realistic ion-atom collision. However, as the impact speed $v_p$ approaches the orbital electron speed $v_e$, the passing projectile ion will have appreciable influence over the electron and thus strongly distort the electron wave function. This mandates use of a more accurate higher order theory to evaluate differential cross sections at lower impact energies. For a $p+H$ collision, when the impact energy is at around $25keV$, $v_p \approx v_e$. At 20 $keV$ impact energy no good agreement to the experiment should be expected from the B1 approximation. Nevertheless, the simplicity of B1 gives us good reason to test our FHBS calculation against it.

To see how to compare an FHBS calculation to an exact B1 calculation, consider the following: in an FHBS calculation the exact matrix element, $S$, is calculated through solving the time-dependent Schrödinger equation. By examining the Liouville-Newmann expansion, we can see this matrix element $S$ is expanded as a power series in the projectile charge $Z_p$:

$$S = Z_p \cdot (B1\ term) + Z_p^2 \cdot (second\ Born\ term) + \ldots \ . \tag{2.1}$$

By setting the charge $Z_p$ to a small value, the contribution from terms other than the first Born is negligible. What we have is

$$S \approx Z_p \cdot (B1\ term), \qquad (Z_p << 1). \tag{2.2}$$

To compare a differential cross section calculate by using the above FHBS method to the one obtained from an exact B1 calculation, we only need to divide the final cross section by a factor of $Z_p^2$. The is because the cross section is proportional to the absolute square of the matrix element.

The FHBS method is a partial wave expansion method. To check an FHBS calculation, one compares it to a B1 calculation using the same number of partial waves. However in the FHBS calculation, the convergence of partial waves is also important. So in this chapter the full-wave B1 approximation calculation is also discussed and its results are compared to the partial wave B1 calculation. We hope the B1 calculation from full wave and a partial wave expansion will partly gives us a hint of how many partial waves are required for an FHBS calculation at the impact energy (20 $keV$) we are considering.

## A. The First Born (B1) Approximation

In this section we are going to work out the expression to calculate the angular distribution in the Born approximation for $p + H$ collision. We follow [13] and work in the wave

function representation. In the Born approximation, the differential cross section is give by

$$d\sigma_{f,i}(\Omega) = \frac{\mu^2}{4\pi^2}\Big| \int \chi_f^*(\mathbf{r}) \frac{Z_p e^{-i\mathbf{Q}\cdot\mathbf{R}}}{|\mathbf{R}-\mathbf{r}|} \chi_i(\mathbf{r})\, d\mathbf{r}\, d\mathbf{R}\Big|^2 d\Omega. \tag{2.3}$$

Here $\mu$ is the reduce mass of the incident proton, $\mathbf{r}$ is the displacement vector from the electron to the nucleus, $\mathbf{R}$ is the displacement vector from the target nucleus to the incident proton, and $\mathbf{Q}$ is the momentum transfer between the initial and final state. $\chi_i(\mathbf{r})$ is the initial state of the electron and $\chi_f(\mathbf{r})$ is the final state after collision. The expression can be simplified by integrating over the coordinates of $\mathbf{R}$. After integration the result is

$$d\sigma_{f,i}(Q) = 8\pi Z_p^2 \frac{1}{v_p^2}\frac{dQ}{Q^3}\Big| \int \chi_f^*(\mathbf{r}) e^{-i\mathbf{Q}\cdot\mathbf{r}} \chi_i(\mathbf{r})\, d\mathbf{r}\Big|^2. \tag{2.4}$$

Here $v_p$ is projectile speed. Eq. (2.4) is used as a starting point in our B1 angular distribution. The expression inside the absolute square is referred to as *form factor*,

$$F_{f,i}(Q) = \int \chi_f^*(\mathbf{r}) e^{-i\mathbf{Q}\cdot\mathbf{r}} \chi_i(\mathbf{r})\, d\mathbf{r}. \tag{2.5}$$

For a $p+H$ collision, $Z_p = 1$. The initial state of the target electron, $\chi_i(\mathbf{r})$, is the $1s$ ground state of the target hydrogen atom $|0>$. The electron will be ionized by the projectile proton into a final state, $\chi_f(\mathbf{r})$, with momentum $\mathbf{k}$. It is the partial wave expansion of the final state $|\mathbf{k}>$ which would give us comparison of the B1 approximation to the FHBS calculation. Both the initial and final wave function satisfy the following Schrödinger equation

$$(-\frac{\Delta}{2} - \frac{1}{r})\ \chi(\mathbf{r}) = E\ \chi(\mathbf{r}). \tag{2.6}$$

The solution to the $1s$ ground state wave function is

$$|0> = 2e^{-r}\, Y_{0,0}. \tag{2.7}$$

There are two solutions for a scattering state with momentum $\mathbf{k}$, namely

$$\chi_{\mathbf{k}}^{(+)}(\mathbf{r}) = e^{\pi/2k}\Gamma(1-i/k)e^{-i\mathbf{k}\cdot\mathbf{r}}F(i/k,1,ikr+i\mathbf{k}\cdot\mathbf{r}) \tag{2.8}$$

$$\chi_{\mathbf{k}}^{(-)}(\mathbf{r}) = e^{\pi/2k}\Gamma(1+i/k)e^{i\mathbf{k}\cdot\mathbf{r}}F(-i/k,1,-ikr-i\mathbf{k}\cdot\mathbf{r}). \tag{2.9}$$

There is a question of which wave function of the above two should be used in the final state in the transition matrix $<\mathbf{k}|e^{-i\mathbf{Q}\cdot\mathbf{r}}|0>$. The answer is the final wave solution should be a plane wave plus an *ingoing* spherical wave [14], which is $\chi_{\mathbf{k}}^{(-)}(\mathbf{r})$ in Eq. (2.9).

In the rest of this sections we examined how to calculate the angular distribution of $p+H$ collision from the *form factor* by using expression (2.9). The next section will describe how to calculate the angular distribution and by using the the partial wave expansion of $\chi_{\mathbf{k}}^{(-)}(\mathbf{r})$. By using expression (2.9) the *form factor* is

$$\begin{aligned} & <\chi_{\mathbf{k}}^{(-)}(\mathbf{r})|e^{-i\mathbf{Q}\cdot\mathbf{r}}|0> \\ = \;& e^{\pi/2k}\Gamma(1-i/k)\int e^{-i\mathbf{k}\cdot\mathbf{r}}F(i/k,1,ikr+i\mathbf{k}\cdot\mathbf{r})e^{-i\mathbf{Q}\cdot\mathbf{r}}2e^{-r}\frac{1}{4\pi}d^3\mathbf{r}. \end{aligned} \tag{2.10}$$

This integral can be performed analytically by using the properties of the Confluent Hypergeometric Function and changing the order of integrals. The complete calculation can be found in [15]. The result is

$$\begin{aligned} & <\chi_{\mathbf{k}}^{(-)}(\mathbf{r})|e^{-i\mathbf{Q}\cdot\mathbf{r}}|0> \\ = \;& \frac{4\cdot e^{\pi/2k}\Gamma(1-i/k)}{(k^2+Q^2+2kQ\cos\gamma+1)^2}\cdot(1-z)^{-(1+i/k)}\Big[2-(1-i/k)\cdot z\Big], \end{aligned} \tag{2.11}$$

where $\gamma$ is the angle between $\mathbf{k}$ and $\mathbf{Q}$ and

$$z = \frac{2k^2+2kQ\cos\gamma+2ik}{k^2+Q^2+2kQ\cos\gamma+1}. \tag{2.12}$$

By using the property of the gamma function

$$\Gamma(1+iy)\Gamma(1-iy) = \frac{\pi y}{\sinh \pi y}, \tag{2.13}$$

we can derive from (2.11) that

$$\begin{aligned} & |<\chi_{\mathbf{k}}^{(-)}(\mathbf{r})|e^{-i\mathbf{Q}\cdot\mathbf{r}}|0>|^2 \\ = \quad & \frac{2^7\pi/k}{1-e^{-2\pi/k}} \cdot \frac{Q^2\cdot[Q^2+2kQ\cos\gamma+(k^2+1)\cos^2\gamma]e^{-\frac{2}{k}tan^{-1}\frac{2k}{Q^2+1-k^2}}}{(k^2+Q^2+2kQ\cos\gamma+1)^4[(Q^2+1-k^2)^2+4k^2]}. \end{aligned} \tag{2.14}$$

If we are not considering the angular distribution, we simply integrate the above over $d\Omega(\mathbf{k})$ to obtain the total cross section [13], as

$$\sigma_{total} = \frac{8\pi a_0^2}{\eta_s}\int_{W_{min}}^{W_{max}} dW \int_{Q_{min}}^{\infty}\frac{dQ}{Q^3}\int |<\chi_{\mathbf{k}}^{(-)}(\mathbf{r})|e^{-i\mathbf{Q}\cdot\mathbf{r}}|0>|^2 d\Omega(\mathbf{k}). \tag{2.15}$$

Here $W = k^2+1$, where $k$ is the magnitude of the electron momentum. $W_{min} = 1$, and $Q_{min}^2 = \frac{W^2}{4\eta_s}$. For practical purpose $W_{max}$ is set to infinity. The quantity $\eta_s$ is determined by

$$\eta_s = v_p^2. \tag{2.16}$$

For $p+H$ at $20keV$ impact energy, $\eta_s = 0.8$.

To consider the angular distribution, the $d\Omega(\mathbf{k})$ integration is separated into two parts, as $d\Omega(\mathbf{k}) = \sin\theta_k d\theta_k d\phi$. The $d\theta_k$ integration is postponed until we have integrated over $dQ$ and $dW$. By changing the order, the new integration scheme is

$$\sigma_{total} = \frac{8\pi a_0^2}{\eta_s}\int \sin\theta_k d\theta_k \int_{W_{min}}^{W_{max}} dW \int_{Q_{min}}^{\infty}\frac{dQ}{Q^3}\int |<\chi_{\mathbf{k}}^{(-)}(\mathbf{r})|e^{-i\mathbf{Q}\cdot\mathbf{r}}|0>|^2 d\phi. \tag{2.17}$$

The change in integration makes it necessary to modify the $dQ$ integration, because we now need the angular information in $\mathbf{Q}$. The vector $\mathbf{Q}$ is splitted into two parts, one in the

$z$ direction with magnitude $Q_z$ and one in the x-y plane with magnitude $Q_b$. They satisfy

$$Q^2 = Q_b^2 + Q_z^2. \tag{2.18}$$

$Q_z$ is calculated once given W, as

$$Q_z^2 = \frac{W}{4\eta_s}. \tag{2.19}$$

The value of $Q_z$ given by Eq. (2.19) is also the minimum value of $Q$. The $dQ/Q^3$ integration could be translated into a $dQ_b$ integration. To do this, we differentiate Eq. (2.18) and obtain

$$QdQ = Q_b dQ_b. \tag{2.20}$$

In the above we used the fact that $Q_z$ is a fixed value. Thus the integration over $dQ/Q^3$ can be replaced as

$$dQ/Q^3 = Q_b dQ_b/Q^4. \tag{2.21}$$

The final version of the modified integration scheme is

$$\sigma_{total} = \frac{8\pi a_0^2}{\eta_s} \int \sin\theta_k d\theta_k \int_{W_{min}}^{W_{max}} dW \int_0^\infty \frac{Q_b dQ_b}{Q^4} \int |<\chi_{\mathbf{k}}^{(-)}(\mathbf{r})|e^{-i\mathbf{Q}\cdot\mathbf{r}}|0>|^2 d\phi. \tag{2.22}$$

Below we discuss the integration of $|<\chi_{\mathbf{k}}^{(-)}(\mathbf{r})|e^{-i\mathbf{Q}\cdot\mathbf{r}}|0>|^2$ over $d\phi$. In the expression Eq. (2.14) the part which depends on the angle is

$$g(\gamma) = \frac{Q^2 + 2kQ\cos\gamma + (k^2+1)\cos^2\gamma}{(k^2+Q^2+2kQ\cos\gamma+1)^4}. \tag{2.23}$$

Here $\cos\gamma = \cos(\hat{\mathbf{k}}\cdot\hat{\mathbf{Q}})$. In the following we are going to use the addition theorem. Since $\phi$ is the angle between $\mathbf{k}$, $\mathbf{Q}$ in the x-y plane, the addition theorem states that

$$\cos\gamma = \cos\theta_k\cos\theta_Q + \sin\theta_k\sin\theta_Q\cos\phi. \tag{2.24}$$

Given $Q$ and $Q_z$, the value of $\cos\theta_Q$ is calculated as

$$\cos\theta_Q = Q_z/Q, \tag{2.25}$$

and $\sin\theta_Q = \sqrt{1-\cos^2\theta_Q}$, since $\theta_Q$ is within $[0,\pi]$. In the following let $x = \cos\theta_k\cos\theta_Q$, $y = \sin\theta_k\sin\theta_Q$, and rewrite Eq (2.23) as

$$g(\gamma) = \frac{c_1 + c_2\cos\phi + c_3\cos^2\phi}{[a+b\cos\phi]^4}, \tag{2.26}$$

where

$$\begin{aligned} a &= k^2 + Q^2 + 1 + 2kQx \\ b &= 2kQy \\ c_1 &= Q^2 + 2kQx + (k^2+1)\cdot x^2 \\ c_2 &= 2kQy + (k^2+1)\cdot 2xy \\ c_3 &= (k^2+1)\cdot y^2. \end{aligned} \tag{2.27}$$

To finish the integration over $d\phi$, we will need this integral (see Eq. 4.3.133 on page 78 of [16])

$$\int \frac{dz}{a+b\cos z} = \frac{2}{(a^2-b^2)^{\frac{1}{2}}}\arctan\frac{(a-b)\tan\frac{z}{2}}{(a^2-b^2)^{\frac{1}{2}}} \quad (a^2 > b^2), \tag{2.28}$$

which gives

$$I(a,b) = \int_0^\pi \frac{dz}{a+b\cos z} = \frac{\pi}{(a^2-b^2)^{\frac{1}{2}}}. \tag{2.29}$$

Through differentiating $I(a,b)$ we obtain the following:

$$\begin{aligned}
\int_0^\pi \frac{dz}{(a+b\cos z)^4} &= -\frac{1}{6}\frac{\partial^3}{\partial a^3} I(a,b) = \frac{\pi(a^3+\frac{3}{2}ab^2)}{(a^2-b^2)^{\frac{7}{2}}}, \\
\int_0^\pi \frac{\cos z dz}{(a+b\cos z)^4} &= -\frac{1}{6}\frac{\partial^3}{\partial b \partial a^2} I(a,b) = \frac{\pi(2a^2b+\frac{1}{2}b^3)}{(a^2-b^2)^{\frac{7}{2}}}, \\
\int_0^\pi \frac{\cos^2 z dz}{(a+b\cos z)^4} &= -\frac{1}{6}\frac{\partial^3}{\partial b^2 \partial a} I(a,b) = \frac{\pi(\frac{1}{2}a^3+2ab^2)}{(a^2-b^2)^{\frac{7}{2}}}.
\end{aligned} \tag{2.30}$$

Since $g(\gamma)$ is an function of $\cos\phi$, as a function of $\phi$ it is even with respect to $\pi$. This means

$$\int_0^{2\pi} g(\gamma)\, d\phi = 2 \cdot \int_0^\pi g(\gamma)\, d\phi. \tag{2.31}$$

The $d\phi$ integration is done with the help of the integrals in (2.30). The result is

$$\int_0^{2\pi} g(\gamma)\, d\phi = \frac{2\pi}{(a^2-b^2)^{\frac{7}{2}}}\left[c_1(a^3+\frac{3}{2}ab^2) - c_2(2a^2b+\frac{b^3}{2}) + c_3(\frac{a^3}{2}+2ab^2)\right]. \tag{2.32}$$

Eq. (2.32) is the expression we need to calculate the angular distribution.

## B. Partial Wave Expansion

The partial wave expansion is a familiar method in the collision theory. Take the polar axis in the direction of wave vector **k**, a wave function can be expanded into a series of Legendre polynomials:

$$|\mathbf{k}> = \sum_l \chi_l(kr) P_l(\cos\theta). \tag{2.33}$$

Here $\theta$ is angle between **k** and **r**. The partial wave expansion is particularly convenient for central potentials. By taking advantage of the symmetry of a central potential, it is easy to separate radial and angular part of the Schrödinger equation. This usually reduces the problem into solving an one-dimension radial differential equation.

The B1 approximation in the partial wave expansion is through expanding the wave

function $\chi_{\mathbf{k}}^{(-)}(\mathbf{r})$ in the *form factor* $< \chi_{\mathbf{k}}^{(-)}(\mathbf{r})|e^{-i\mathbf{Q}\cdot\mathbf{r}}|0 >$ as the sum of the partial waves. In the partial wave expansion,

$$|\chi_{\mathbf{k}}^{(+)}(\mathbf{r}) >= \sum_{l=0}^{\infty} R_l(kr)P_l(\mathbf{k}\cdot\mathbf{r}), \tag{2.34}$$

where $R_l(kr) = C_l \cdot r^l \cdot e^{ikr} \cdot F(l+1+in, 2l+2, -2ikr)$ and

$$C_l = \frac{(2ik)^l \cdot e^{-\frac{1}{2}n\pi} \cdot \Gamma(l+1+in)}{(2l)!}. \tag{2.35}$$

The form factor can be expressed as

$$< \chi_{\mathbf{k}}^{(-)}(\mathbf{r})|e^{-i\mathbf{Q}\cdot\mathbf{r}}|0 >= \int \sum_{l=0}^{\infty} R_l(kr)P_l(-\mathbf{k}\cdot\mathbf{r}) \cdot e^{-i\mathbf{Q}\cdot\mathbf{r}} \cdot 2e^{-r} \cdot Y_{0,0} \cdot d\mathbf{r} \tag{2.36}$$

Note the expression for the final state wave function is $R_l(kr)P_l(-\mathbf{k}\cdot\mathbf{r})$. The explanation is given in literature [17]. Simply put, the final state wave function $|\chi_{\mathbf{k}}^{(-)}(\mathbf{r}) >$ should asymptotically behave like a plane wave plus an incoming wave. This is obtained by taking the complex conjugate and inverting the direction of momentum of the wave function, $|\chi_{\mathbf{k}}^{(+)}(\mathbf{r}) >$, which behaves asymptotically like plane wave plus an *outgoing* wave. Since the final state $|\chi_{\mathbf{k}}^{(-)}(\mathbf{r}) >$ is on the right side of the matrix element, we only change the direction of the momentum from $\mathbf{k}$ to $-\mathbf{k}$ in the $|\chi_{\mathbf{k}}^{(+)}(\mathbf{r}) >$ expression in Eq (2.34).

We then expand $e^{-i\mathbf{Q}\cdot\mathbf{r}}$ into partial waves

$$e^{-i\mathbf{Q}\cdot\mathbf{r}} = \sum_{l=0}^{\infty} i^l(2l+1)\, j_l(Qr)P_l(-\mathbf{Q}\cdot\mathbf{r}) \tag{2.37}$$

and substitute into the $formfactor$ expression which gives

$$\begin{aligned} & < \chi_{\mathbf{k}}^{(-)}(\mathbf{r}) | e^{-i\mathbf{Q}\cdot\mathbf{r}} | 0 > \\ = & \int \sum_{l=0}^{\infty} C_l \cdot r^l \cdot e^{ikr} \cdot F(l+1+in, 2l+2, -2ikr) \cdot P_l(-\mathbf{k}\cdot\mathbf{r}) \\ & \cdot \sum_{l'=0}^{\infty} i^{l'}(2l'+1) j_{l'}(Qr) P_{l'}(-\mathbf{Q}\cdot\mathbf{r}) \cdot 2e^{-r} \frac{1}{\sqrt{4\pi}} \cdot r^2 dr \cdot d\Omega_{\mathbf{r}}. \end{aligned} \tag{2.38}$$

Note that $P_l(-\cos\theta) = (-1)^l P_l(\cos\theta)$. By applying the addition theorem to both $P_l(\mathbf{k}\cdot\mathbf{r})$ and $P_l(\mathbf{Q}\cdot\mathbf{r})$ (note the difference in the complex conjugate applied for each case):

$$P_l(\mathbf{k}\cdot\mathbf{r}) = \frac{4\pi}{2l+1} \sum_{m=-l}^{l} Y_{lm}^*(\mathbf{r}) Y_{lm}(\mathbf{k}) \tag{2.39}$$

$$P_l(\mathbf{Q}\cdot\mathbf{r}) = \frac{4\pi}{2l+1} \sum_{m=-l}^{l} Y_{lm}^*(\mathbf{Q}) Y_{lm}(\mathbf{r}). \tag{2.40}$$

Integrating over $d\Omega_{\mathbf{r}}$ gives delta functions

$$\int Y_{l,m}^*(\mathbf{r}) Y_{l',m'}(\mathbf{r})\, d\Omega_{\mathbf{r}} = \delta_{l,l'}\delta_{m,m'} \tag{2.41}$$

which eliminate the sum over one $l'$ and $m'$ in Eq. (2.38), thus

$$\begin{aligned} & < \chi_{\mathbf{k}}^{(-)}(\mathbf{r}) | e^{-i\mathbf{Q}\cdot\mathbf{r}} | 0 > \\ = & \sum_{l=0}^{\infty} \int_0^{\infty} C_l \cdot r^l \cdot e^{ikr} \cdot F(l+1+in, 2l+2, -2ikr) \cdot i^l(2l+1) \cdot j_l(Qr) \\ & \cdot (-1)^l \cdot \frac{2e^{-r}}{\sqrt{4\pi}} \cdot r^2 dr (-1)^l \frac{(4\pi)^2}{(2l+1)^2} \sum_{m=-l} Y_{lm}^*(\mathbf{Q}) Y_{lm}(\mathbf{k}). \end{aligned} \tag{2.42}$$

Define integral

$$I_l(k,Q) = \int_0^{\infty} r^l \cdot e^{ikr} \cdot F(l+1+in, 2l+2, -2ikr) \cdot j_l(Qr) \cdot e^{-r} \cdot r^2\, dr. \tag{2.43}$$

After simplifying Eq (2.42) we have

$$< \chi_{\mathbf{k}}^{(-)}(\mathbf{r})|e^{-i\mathbf{Q}.\mathbf{r}}|0 >= \sum_{l=0}^{\infty} C_l \cdot i^l \frac{2}{\sqrt{4\pi}} \cdot I_l(k,Q) \frac{(4\pi)^2}{(2l+1)} \sum_{m=-l} Y_{lm}^*(\mathbf{Q}) Y_{lm}(\mathbf{k}). \qquad (2.44)$$

It is worth pointing out that the result of the integral $I_l(k,Q)$ is real, although it contains complex terms in the integrand. This is because within the integration Eq. (2.43) there are only two complex terms. The product of these two complex terms, $e^{ikr} \cdot F(l+1+in, 2l+2, -2ikr)$, is real (proof see [15]). This simplifies further treatment of the phase which will be discussed later.

In the following we concentrate on calculating the integral of $I_l(k,Q)$. Our derivation shows the integral needs to be treated separately for $l=0$ and $l>0$. For $l=0$,

$$I_0(k,Q) = \int_0^{\infty} e^{ikr} \cdot F(1+in, 2, -2ikr) \cdot j_0(Qr) \cdot e^{-r} \cdot r^2 \, dr. \qquad (2.45)$$

Making use of the zero'th *Bessel function* expression $j_0(Qr) = \frac{\sin Qr}{Qr}$, and $\sin Qr = \frac{e^{iQr} - e^{-iQr}}{2i}$, one have

$$\begin{aligned} & I_0(k,Q) \\ = & \frac{1}{2iQ} \int_0^{\infty} e^{ikr} F(1+in, 2, -2ikr)(e^{iQr} - e^{-iQr}) e^{-r} r dr \\ = & \frac{1}{2iQ} \int_0^{\infty} (e^{-[1-i(k+Q)]r} - e^{-[1-i(k-Q)]r}) F(1+in, 2, -2ikr) r dr. \end{aligned} \qquad (2.46)$$

If we examine the integrals with two terms in the bracket, we will find both are standard integrals involving the Hyper-geometric Function in the form of

$$\int_0^{\infty} e^{-\lambda z} z^{\nu} F(\alpha, \gamma, kz) dz = \Gamma(\nu+1) \lambda^{-\nu-1} F(\alpha, \nu+1, \gamma, k/\lambda). \qquad (2.47)$$

Applying this result only to the integral with the first term gives

$$\begin{aligned} & \int_0^\infty e^{-[1-i(k+Q)]r} F(1+in,2,-2ikr) r dr \\ = \;& \Gamma(2) \left( \frac{1}{a_0} - ik - iQ \right)^{-2} F(1+in,2,2,\frac{-2ik}{1-ik-iQ}). \end{aligned} \tag{2.48}$$

This expression can be further simplified by the following property of Confluent Hypergeometric Function (see Eq15.3.3 of [16])

$$F(a,b;c;z) = (1-z)^{c-a-b} F(c-a,c-b;c;z), \tag{2.49}$$

which leads to

$$\begin{aligned} & F(1+in,2,2,\frac{-2ik}{1-ik-iQ}) \\ = \;& \left( 1 - \frac{-2ik}{1-ik-iQ} \right)^{-(1+in)} \\ = \;& \left( \frac{1+ik-iQ}{1-ik-iQ} \right)^{-(1+in)}. \end{aligned} \tag{2.50}$$

The result for the integral with the first term in Eq. (2.46) for $I_0(k,Q)$ is

$$\begin{aligned} & \int_0^\infty e^{-[1-i(k+Q)]r} F(1+in,2,-2ikr) r dr \\ = \;& \frac{1}{(1-ik-iQ)^{1-in}} \frac{1}{(1+ik-iQ)^{1+in}}. \end{aligned} \tag{2.51}$$

Replace $Q$ with $-Q$ in the above expression will give the result to the integral with the second term. The answer to $I_0(k,Q)$ is

$$\begin{aligned} I_0(k,Q) \;=\; & \frac{1}{2iQ} \left[ \frac{1}{(1-ik-iQ)^{1-in}} \frac{1}{(1+ik-iQ)^{1+in}} \right. \\ & \left. - \frac{1}{(1-ik+iQ)^{1-in}} \frac{1}{(1+ik+iQ)^{1+in}} \right]. \end{aligned} \tag{2.52}$$

The two terms in the above expression are complex conjugate to each other, as it is easy to verify that

$$\begin{aligned} & \left[\frac{1}{(1-ik+iQ)^{1-in}}\frac{1}{(1+ik+iQ)^{1+in}}\right]^* \\ = \quad & \frac{1}{(1-ik-iQ)^{1-in}}\frac{1}{(1+ik-iQ)^{1+in}}. \end{aligned} \tag{2.53}$$

Since it is the subtraction of the two complex conjugate terms, the expression for $I_0(k,Q)$ should be

$$I_0(k,Q) = \frac{1}{Q} Imag\left[\frac{1}{(1-ik-iQ)^{1-in}}\frac{1}{(1+ik-iQ)^{1+in}}\right], \tag{2.54}$$

which is real as expected.

To calculate $I_l(k,Q)$ for $l>0$', first let us use the integral form of the *Confluent Hypergeometric Function*

$$\begin{aligned} & F(l+1+in,2l+2,-2ikr) \\ = \quad & \frac{\Gamma(2l+2)}{\Gamma(l+1+in)\Gamma(l+1-in)}\int_0^1 e^{-2ikrt}\cdot t^{l+in}\cdot(1-t)^{l-in}dt. \end{aligned} \tag{2.55}$$

Change the order of integration in $I_l(k,Q)$ and use the above integral gives

$$\begin{aligned} I_l(k,Q) = \quad & \frac{\Gamma(2l+2)}{\Gamma(l+1+in)\Gamma(l+1-in)}\int_0^1 t^{l+in}\cdot(1-t)^{l-in}dt \\ & \cdot\int_0^\infty r^{l+2}\cdot j_l(Qr)\cdot e^{-[1+i(2t-1)k]r}\,dr \end{aligned} \tag{2.56}$$

By applying the association $j_l(\rho)=\sqrt{\frac{1}{2}\pi/\rho}J_{l+\frac{1}{2}}(\rho)$ and the following integral (see Eq. 6.623 on Page 712 of [18])

$$\int_0^\infty e^{-\alpha x}\,J_\nu(\beta x)\,x^{\nu+1}dx = \frac{2\alpha(2\beta)^\nu\Gamma(\nu+\frac{3}{2})}{\sqrt{\pi}(\alpha^2+\beta^2)^{\nu+\frac{3}{2}}} \quad (Re\nu>-1, Re\alpha>|Im\beta|) \tag{2.57}$$

we obtain the result of the $dr$ integral

$$\int_0^\infty r^{l+2}\cdot j_l(Qr)\cdot e^{-[1+i(2t-1)k]r}\cdot\ dr=\sqrt{\frac{1}{2}\pi/(Q)}\frac{2\alpha(2Q)^{l+\frac{1}{2}}\Gamma(l+2)}{\sqrt{\pi}(\alpha^2+Q^2)^{l+2}}, \tag{2.58}$$

where $\nu=l+\frac{1}{2}>-1,\ \alpha=1+i(2t-1)k$ and $Re\alpha=1>Re\beta=|ImQ|=0$ so all the conditions are satisfied. Our final expressions for $I_l(k,Q)$ is

$$\begin{aligned} I_l(k,Q) &= \frac{\Gamma(2l+2)\Gamma(l+2)}{\Gamma(l+1+in)\Gamma(l+1-in)}\cdot 2^{l+1}Q^l \\ &\quad\cdot\int_0^1 t^{l+in}\cdot(1-t)^{l-in}\cdot\frac{1+i(2t-1)k}{([1+i(2t-1)k]^2+Q^2)^{l+2}}dt. \end{aligned} \tag{2.59}$$

For k large and n is small (note $n=-1/k$) we can do this integration by a straight Gaussian integration and some observation of the integrand. By change of variables as $t=1-x$, we can prove that

$$\begin{aligned} &\int_0^x t^{l+in}\cdot(1-t)^{l-in}\cdot\frac{1+i(2t-1)k}{([1+i(2t-1)k]^2+Q^2)^{l+2}}dt \\ =\ &\left[\int_{1-x}^1 t^{l+in}\cdot(1-t)^{l-in}\cdot\frac{1+i(2t-1)k}{([1+i(2t-1)k]^2+Q^2)^{l+2}}dt\right]^*. \end{aligned} \tag{2.60}$$

Let $x=\frac{1}{2}$, we will see for the above integral

$$\int_0^1=\int_0^{\frac{1}{2}}+\int_{\frac{1}{2}}^1=2\cdot real[\int_0^{\frac{1}{2}}]. \tag{2.61}$$

This means we only need to integrate over (0, 1/2). However, for small k values, $n=-1/k$ is big, the integrand in the above integral is highly oscillating due to the terms of $t^{l+in}$ and $(1-t)^{l-in}$. Direct Gaussian integration won't guarantee convergence. The solution is to expand the function

$$f(t)=\frac{1+i(2t-1)k}{([1+i(2t-1)k]^2+Q^2)^{l+2}} \tag{2.62}$$

into a Taylor series of $(1-2t)$. For convenience, let $x=ik(1-2t)$, and let $f^{(m)}(x)$ be the

m'th differentiation of

$$f(x) = \frac{1-x}{[(1-x)^2+Q^2]^{l+2}} \tag{2.63}$$

to the variable $x$. The Taylor series of $f(t)$ is

$$f(t) = \sum_{m=0}^{\infty} \frac{f^{(m)}(0)}{m!}(ik)^m(1-2t)^m. \tag{2.64}$$

Thus

$$\begin{aligned} & \int_0^1 t^{l+in}\cdot(1-t)^{l-in}\cdot f(t)\cdot dt \\ = & \sum_{m=0}^{\infty}\frac{f^{(m)}(0)}{m!}(ik)^m\int_0^1 t^{l+in}\cdot(1-t)^{l-in}\cdot(1-2t)^m\,dt. \end{aligned} \tag{2.65}$$

The integral in the above sum is a Hyper-geometric Function. Let $a=-m$, $b=l+1+in$, $c=2l+2$ and $z=2$, the integral

$$\begin{aligned} & \int_0^1 t^{l+in}\cdot(1-t)^{l-in}\cdot(1-2t)^m\cdot dt \\ = & \frac{\Gamma(l+1+in)\Gamma(l+1-in)}{\Gamma(2l+2)}F(-m,l+1+in;2l+2;2). \end{aligned} \tag{2.66}$$

It turns out the series expansion of the above Hyper-geometric Function is finite, as

$$F(-m,l+1+in;2l+2;2) = \sum_{i=0}^{m}\frac{(a)_i(b)_i}{(c)_i}\frac{z^n}{n!} \tag{2.67}$$

where $(a)_0=1$ and $(a)_i = a\cdot(a+1)\cdot...(a+i-1)$, etc. So the integral

$$\begin{aligned} & \int_0^1 t^{l+in}\cdot(1-t)^{l-in}\cdot f(t)\cdot dt \\ = & \frac{\Gamma(l+1+in)\Gamma(l+1-in)}{\Gamma(2l+2)}\sum_{m=0}^{\infty}\frac{f^{(m)}(0)}{m!}(ik)^m\sum_{i=0}^{m}\frac{(a)_i(b)_i}{(c)_i}\frac{z^n}{n!} \end{aligned} \tag{2.68}$$

and the series expansion of $I_l(k,Q)$ is

$$I_l(k,Q) \;=\; \Gamma(l+2)\cdot 2^{l+1}Q^l \sum_{m=0}^{\infty} \frac{f^{(m)}(0)}{m!}(ik)^m \sum_{i=0}^{m} \frac{(a)_i (b)_i}{(c)_i}\frac{z^n}{n!}, \tag{2.69}$$

where as noted elsewhere $a=-m$, $b=l+1+in$, $c=2l+2$ and $z=2$.

Numerical calculation shows that for $k>0.2$, we could use the Gaussian integration scheme; for $k<0.2$, the Taylor expansion method works well using up to 10'th Taylor expansion ($m_{max}=10$). Both methods give almost same result when $k=0.2$ in the worst case (Q=0.0) and the relative difference is less than 0.1 percent.

Once $I_l(k,Q)$ is calculated one can integrate over $d\phi$ to obtain the angular distribution over the $\theta_k$. In the following let $\varepsilon_l = C_l \cdot i^l \frac{2}{\sqrt{4\pi}} \cdot I_l(k,Q)\frac{(4\pi)^2}{(2l+1)}$. The *spherical harmonics* are related to *associated Legendre polynomials* by

$$Y_{lm}(\theta,\phi) = \sqrt{\frac{2l+1}{4\pi}\frac{(l-m)!}{(l+m)!}}P_l^m(\cos\theta)\; e^{im\phi}. \tag{2.70}$$

Since $\int_0^{2\pi} e^{-im'\phi}e^{im\phi}d\phi = 2\pi\;\delta_{m,m'}$ we have

$$\begin{aligned}
&\int_0^{2\pi} |<\chi_{\mathbf{k}}^{(-)}(\mathbf{r})|e^{-i\mathbf{Q}.\mathbf{r}}|0>|^2 d\phi_k \\
=\;& \int_0^{2\pi} \sum_{l=0}^{\infty}\varepsilon_l \sum_{m=-l} Y_{lm}^*(\mathbf{Q})Y_{lm}(\mathbf{k}) \sum_{l'=0}^{\infty}\varepsilon_{l'}^* \sum_{m'=-l'} Y_{l'm'}(\mathbf{Q})Y_{l'm'}^*(\mathbf{k})d\phi_k \\
=\;& 2\pi\sum_{l,l'}^{\infty}\varepsilon_l\varepsilon_{l'}^* \sum_{m=-l}^{l} Y_{lm}^*(\mathbf{Q})\sqrt{\frac{2l+1}{4\pi}\frac{(l-|m|)!}{(l+|m|)!}}P_l^{|m|}(\cos\theta_k) \\
& Y_{l'm}(\mathbf{Q})\sqrt{\frac{2l'+1}{4\pi}\frac{(l'-|m|)!}{(l'+|m|)!}}P_{l'}^{|m|}(\cos\theta_k).
\end{aligned} \tag{2.71}$$

In Eq. (2.71) the $m$ value in $Y_{lm}^*(\mathbf{Q})$ and $Y_{l'm}(\mathbf{Q})$ are the same. This leads to the cancellation of the exponential factor $e^{im\phi_Q}$. This means the above is not an function of $\phi_Q$. We can proceed the integration to obtain angular distribution as described in Eq. (2.22). The value of $\cos\theta_Q$ is calculated in Eq. (2.25).

We shall now discuss the phase calculation in $\varepsilon_l$. For $l = 0$, we first calculate the magnitude of $c_0 = e^{-\frac{1}{2}n\pi}\Gamma(1+in)$. Using the property of the *Gamma Function* as in Eq (2.13), we have

$$c_0 \cdot c_0^* = e^{-n\pi}\Gamma(1-in)\Gamma(1+in) = \frac{2n\pi}{e^{2n\pi}-1}. \tag{2.72}$$

This gives

$$\varepsilon_0 = \frac{(4\pi)^2}{\sqrt{\pi}} \cdot c_0 I_0(k,Q) = \frac{(4\pi)^2}{\sqrt{\pi}} \cdot \sqrt{\frac{2n\pi}{e^{2n\pi}-1}} \cdot I_0(k,Q) \cdot phase, \tag{2.73}$$

where the *phase* is from the gamma function but can be ignored in the calculation. To see this, examine the expression of $c_l$ for $l > 0$ (2.35),

$$\varepsilon_l = \frac{(2k)^l \cdot i^l e^{-\frac{1}{2}n\pi}\Gamma(l+1+in)}{(2l)!} \cdot i^l \frac{2}{\sqrt{4\pi}} \cdot I_l(k,Q) \frac{(4\pi)^2}{(2l+1)}. \tag{2.74}$$

From $\Gamma(l+z) = z\,\Gamma(z)$ we can derive $\Gamma(l+1+in) = (l+in)...(1+in)\Gamma(1+in)$. After simplification and rearrangement of terms we have

$$\varepsilon_l = (-1)^l \frac{(2k)^l \cdot I_l(k,Q)(4\pi)^2}{(2l+1)!\sqrt{\pi}} \cdot e^{-\frac{1}{2}n\pi} \cdot \Gamma(1+in)(l+in)...(1+in). \tag{2.75}$$

If we notice $c_0 = e^{-\frac{1}{2}n\pi}\Gamma(1+in)$ this would be

$$\varepsilon_l = (-1)^l \frac{(2k)^l \cdot I_l(k,Q) \cdot (4\pi)^2}{(2l+1)!\sqrt{\pi}} \cdot |c_0| \cdot (l+in)...(1+in) \cdot phase, \tag{2.76}$$

where the *phase* is the very same phase as in the expression of $\varepsilon_0$. In expression (2.71) every $\varepsilon_l$ has this same phase, and every $\varepsilon_l$ is paired with $\varepsilon_{l'}^*$, the complex conjugate of $\varepsilon_{l'}$. This effectively cancels the common phase factor mentioned above. It is just a transient factor; no detailed calculation is necessary.

C. Convergence of the Partial Waves in the First Born Calculation

In the above two sections we described two B1 methods of computing the angular distribution for a $p+H$ collision. The first method is to use the full wave function for the final state $|\mathbf{k}>$ in the matrix element. The second method is to expand this wave function $|\mathbf{k}>$ in a partial waves. Both methods are programmed into FORTRAN code. The Gaussian integration scheme is adopted for the $dQ_b$ and $dW$ integration.

Numerical calculations using both method are carried out at $20keV$ and $48keV$ impact energies. For the partial wave expansion four results are listed: partial wave channel results including $s$ to $d$, $s$ to $f$, $s$ to $g$, and $s$ to $h$, respectively, as shown in Table II. As far as total cross sections are concerned, the partial wave results quickly converge to the whole wave calculation. The $s-d$ partial wave already make up almost two thirds of the total contribution at both 20 keV and 48 keV. The difference quickly diminishes as more partial waves are included. The percentage difference is less than 0.5% for 20 keV projectile energy and less than 2% for 48 keV projectile energy after $h$ partial waves are included.

Table II. Total Cross Sections from Two B1 Methods

| | s-d | s-f | s-g | s-h | All-Partial Wave |
|---|---|---|---|---|---|
| 20 keV | 1.95 | 2.06 | 2.09 | 2.10 | 2.11 |
| 48 keV | 1.69 | 1.83 | 222 | 1.89 | 1.91 |

In Fig. 1 and Fig. 2 we plot out the angular differential cross sections at projectile energy 20 keV and 48 keV. We again notice a rapid convergence of the partial wave results to the full wave results. For the partial wave calculation, in the large angle region the angular differential cross section is usually *higher* than the full wave cross section. It is decreased by adding more partial wave channels to the calculation. At forward angles the partial wave cross sections are always lower, and keep increasing as more partial waves

are added. The difference between the $s-h$ partial wave calculation and the full wave calculation (labeled as All in the graph) is small.

From the above results we conclude at 20 keV impact energy, a partial waves calculation including $s$ to $h$ partial waves would be sufficient enough to ensure convergence. That is the maximum number of partial waves used in our FHBS calculations.

## D. Comparison of FHBS to B1 approximation

The exact partial wave B1 calculation can be compared to an FHBS calculation, as described in the beginning of this chapter. Fig. 3 shows the angular distribution of ionized electrons calculated by the partial wave B1 method with results obtained from an FHBS Born calculation. The FHBS calculation is carried out using the value $Z_p = 0.01$ in the series expansion of Eq. (2.1). The results are for $s-f$ partial waves.

Fig. 3 shows at small angles the FHBS is comparable to an exact B1 calculation. When the cross section is large the FHBS method has errors up to 10%. However at angles above $120^0$ the method is quite poor with percentage error of more than 20%.

The discrepancy at large angles demonstrates the limitation of the FHBS method in producing the angular distribution of ionized electrons. One possible explanation is the method to determine the phase information, to be described in Chapter IV, are simply not accurate enough. It is also our experience that FHBS usually gives a bigger percentage error for smaller scattering cross sections. This percentage error, coupled with the subtle cancellation when the partial wave amplitudes are summed, might be responsible for the discrepancy at large angles.

The conclusion is the FHBS method is accurate within 10% error for forward scattering angles, but not reliable at large backward scattering angles.

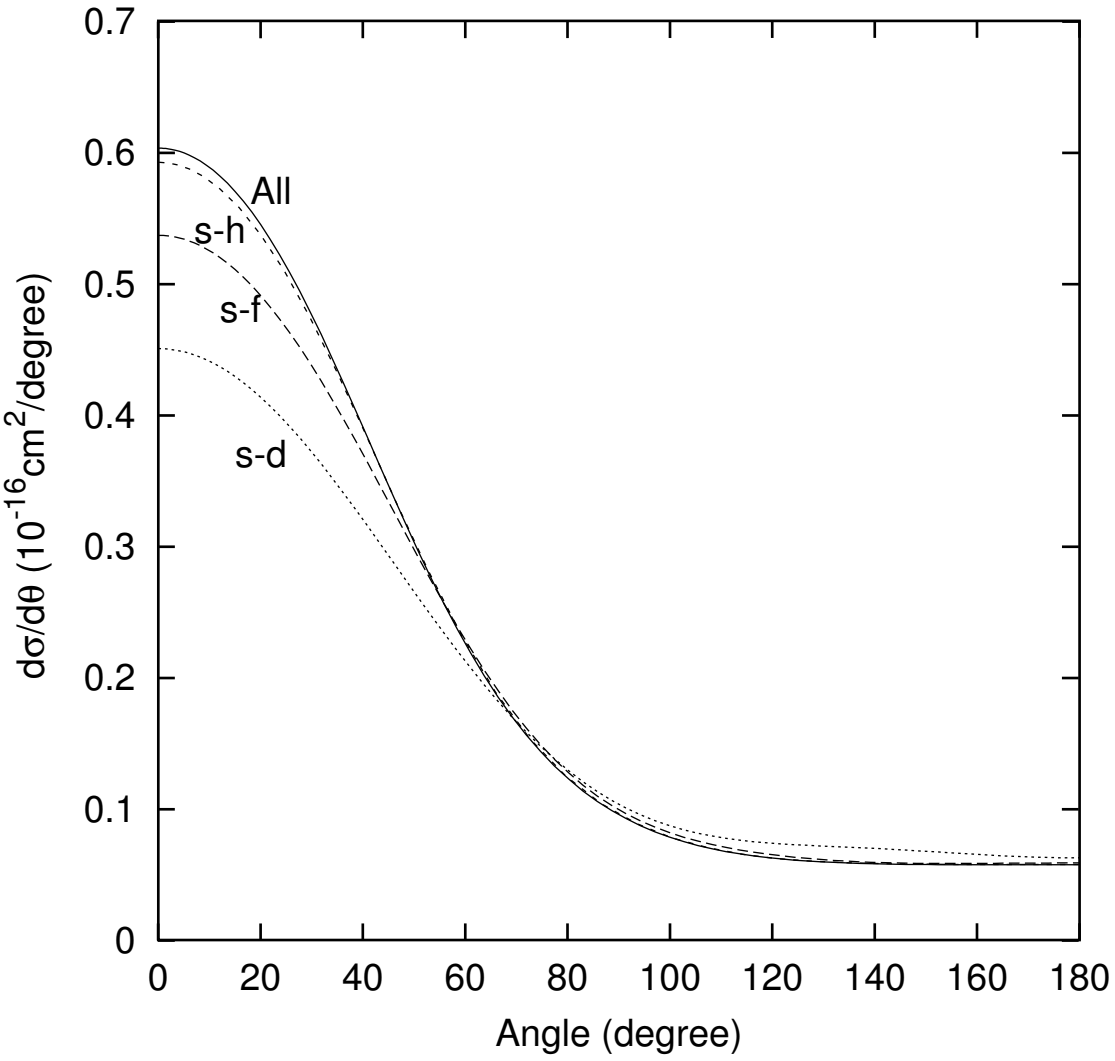


Fig. 1. Angular distribution of electrons at 20 keV projectile impact energy according to B1 calculation for the p+H collision. This shows the convergence of the partial wave calculation to the full wave result.

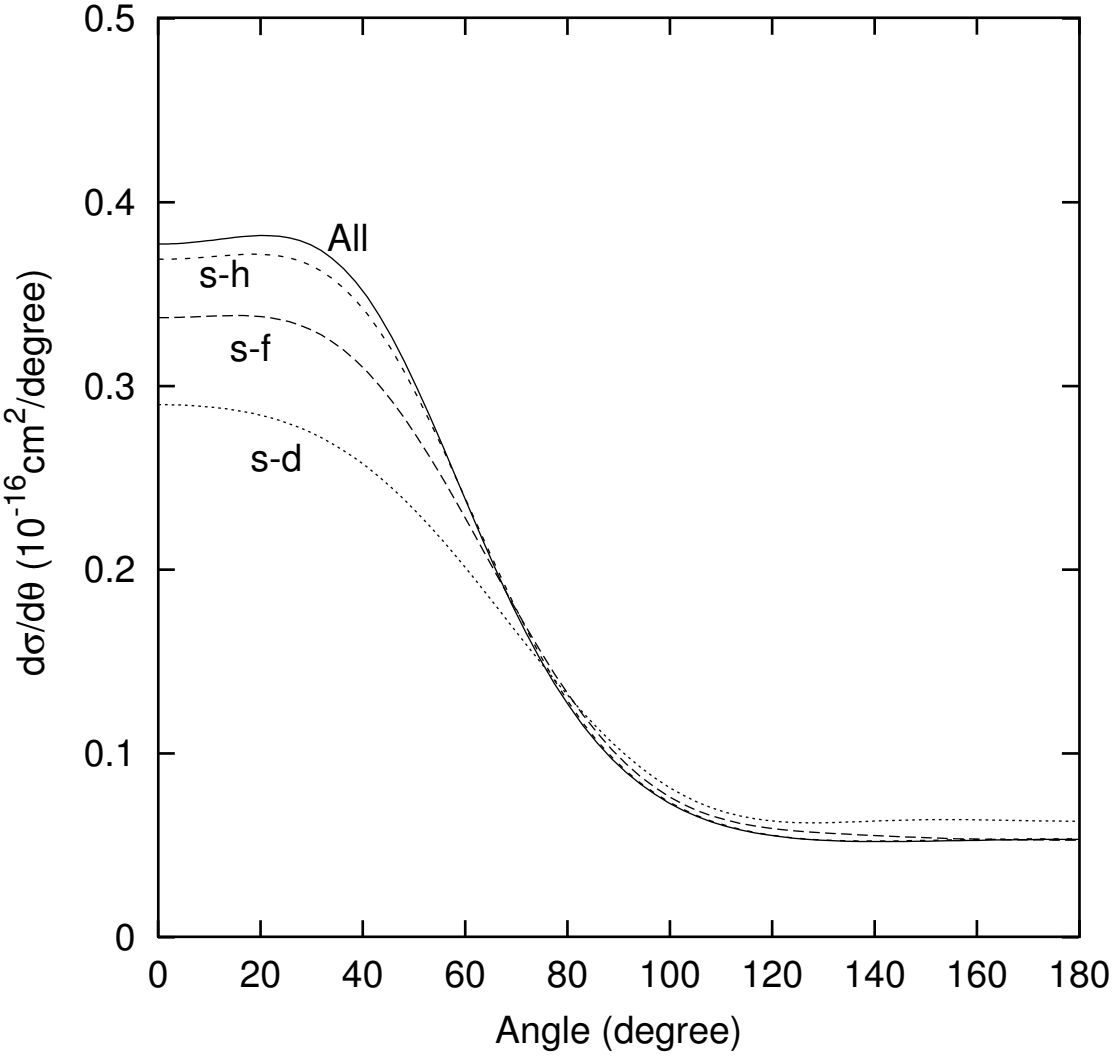


Fig. 2. Angular distribution of electrons at 48 keV projectile impact energy according to B1 calculation for the p+H collision.

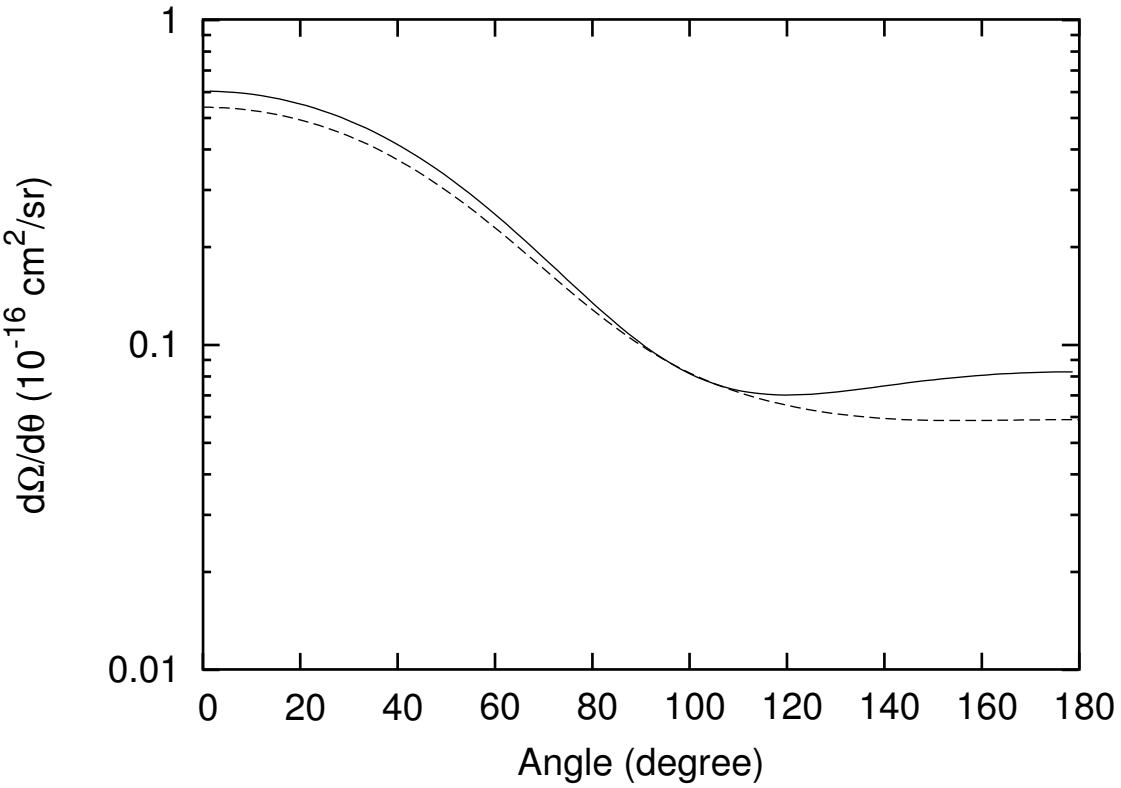


Fig. 3. Comparison of angular distribution given by B1 and FHBS Born in a $p+H$ collision at 20 keV. The exact B1 result is the dotted line and the FHBS born result is the solid line.

# CHAPTER III

# THE FHBS METHOD

The purpose of this chapter is to develop a method to obtain angular and energy differential cross sections in one center (target or projectile) from the coupled-channel Finite Hilbert Basis Set (FHBS) calculation. *Coupled* means intermediate states are included in the calculation, as opposed to no intermediate states in the B1 approximation. The FHBS calculation can be using one of the three methods: SCE, OHCE and TCE. We will not go into the details of each method, but will mainly focus on the procedure in obtaining the angular and energy distribution from a FHBS calculation.

A coupled-channel FHBS calculation begins with preparing a Finite Hilbert Basis Set. The electron states are represented in this basis set. The target or projectile Hamiltonian are diagonized in this basis. There are several considerations in preparing a good basis set. For example a resonance state should be included into the basis to reflect the Thomas mechanism.

The target or projectile Hamiltonian has a kinetic energy part and a potential part. The projection of the kinetic energy part of the Hamiltonian into our Hilbert space discretized the continuum energy spectrum. These discretized eigen-states are called pseudo-states. Transition probabilities to the continuum are calculated by using the pseudo-states through numerically solving the time-dependent Schrödinger equation. To obtain a continuous energy and angular distribution, a connection is established between a pseudo-state and an actual state. To accomplish this, an actual continuum wave function $|\chi(\varepsilon_\lambda)>$, is approximated by a basis state as

$$\mathbf{P}|\chi(\varepsilon_\lambda)>=N_\lambda|\chi_\lambda> .$$

This approximation allows us to obtain the transition amplitude $T$ from the $U$-matrix cal-

culated by a FHBS method. However by using this method the transition amplitudes are limited to the discretized pseudo-state energies. Interpolation is then used to obtain a continuous differential cross section. The validity of this approach is subject to test.

There are three FHBS methods to obtain the $U$-matrix, as described in the Introduction. Here we review each method from the point view of obtaining the ionization differential cross sections.

In the Single-Centered-Expansion (SCE), the wave function of the electron is expanded upon a basis set around the target or projectile, but not both. Sometimes it is referred to as the target-centered SCE or projectile-centered SCE method. The charge transfer channels between the target and projectile are not included in the SCE. This is a shortcoming for the SCE in obtaining differential cross sections at $20keV$, as the charge transfer is important at this impact energy. On the other hand, lack of the charge transfer channels makes the SCE a good candidate to check the ability to obtain differential cross sections with the B1 approximation, since the charge transfer is also not considered in the B1 theory. This check has been presented in Chapter II.

The One-and-Half-Centered-Expansion (OHCE) adds the projectile bound states to the basis. This allows better description of the ionization that leads to charge transfer. In both the OHCE and the SCE method, there is only one continuum basis, which is around the target. The positive energy electron described SCE or OHCE has its momentum represented in the target frame. Thus it simple to obtain differential cross sections in the lab frame in SCE or OHCE. As we have shown [4] OHCE gives a good energy distribution at $48keV$ impact energy. At lower impact energy of $20keV$ the OHCE method show signs of failing. The angular distribution of OHCE at $20keV$ impact energy is presented at the end of this chapter.

The Two-Centered Expansion (TCE) uses two complete basis sets, one centered around target and one centered around the projectile. This way both wave functions around each

center are well represented. As $t \to \infty$, the two centers are far apart and the two basis sets don't overlap with each other. The TCE can not only fully describe the charge transfer between target and projectile as OHCE, but also enhance the ability to steering away electrons by the additional projectile continuum channel.

As far as differential cross sections are concerned, the two continuum basis of TCE brings new difficulties. There are two contributions to the direct ionization, one from the target continuum and one from the projectile continuum. These two contributions need to be included together to obtain differential cross sections. The method is to translate the projectile scattering amplitude into the target frame through a Galilean transformation. However the transformation requires the information of scattering amplitude as a function of momentum $\mathbf{k}'$ in the projectile frame. Thus finding the scattering amplitude as a function of momentum in each respective center is the main task of this chapter. The details of TCE differential cross sections are described in the next chapter.

## A. Semi-Classical Approximation

In the Semi-Classical Approximation, heavy colliding objects like the projectile proton in the $p+H$ collision are assumed to follow a classical trajectory. Recoil of the target is believed to be insignificant. Since the projectile is massive, we further assume there is no deflection for the projectile. The trajectory of the projectile is approximated by a straight line. Let $\mathbf{B}$ be the impact parameter and $\mathbf{v_p}$ be the projectile velocity, the projectile trajectory $\mathbf{R}$ as a function of time $t$ can be described as

$$\mathbf{R}(t) = \mathbf{B} + \mathbf{v_p} t. \tag{3.1}$$

## B. Finite Hilbert Basis Set

The FHBS method uses a set of square-integrable radial functions to represent eigen-states of target and projectile. Examples of such functions are exponentials, Gaussians, etc. In this work a complex exponential basis in the form of $r^l e^{-\alpha r}$ is used to generate state vectors. A basis in this representation is written as

$$\zeta_i = r^l e^{-\alpha_i r} y_{l,m}(\hat{\mathbf{r}}), \tag{3.2}$$

where $l, m$ are angular momentum numbers, and

$$y_{l,m}(\hat{\mathbf{r}}) = \frac{Y_{l,m}(\hat{\mathbf{r}}) + Y^*_{l,m}(\hat{\mathbf{r}})}{\sqrt{2}\sqrt{1+\delta_{m,0}}}. \tag{3.3}$$

In the above expression the $Y_{l,m}(\hat{\mathbf{r}})$'s are *Spherical Harmonics*. Another similar function, to be used later, is defined as

$$\bar{y}_{l,m}(\hat{\mathbf{r}}) = \frac{Y_{l,m}(\hat{\mathbf{r}}) - Y^*_{l,m}(\hat{\mathbf{r}})}{\sqrt{2}\sqrt{1+\delta_{m,0}}}. \tag{3.4}$$

A state vector with energy $E_\lambda$ and angular momentum $l, m$ is expressed as

$$|\chi_\lambda(\mathbf{r})> = \sum_i a(i,\lambda)\zeta_i. \tag{3.5}$$

Here $\lambda$ is the energy index. The coefficients, $a(i,\lambda)$ and $\alpha_i$, are generally complex numbers. Sometimes for convenience we express the radial part of the wave function as

$$\chi_{\lambda,l}(r) = \sum_i a(i,\lambda) r^l e^{-\alpha_i r}. \tag{3.6}$$

The coefficients, $a(i,\lambda)$'s, are chosen to minimize

$$< \chi_\lambda(\mathbf{r})|(H - E_\lambda)|\chi_\lambda(\mathbf{r}) >, \tag{3.7}$$

where $H$ is the Hamiltonian of the target or the projectile. Usually the Hamiltonian has a kinetic energy term and a potential term, as

$$H = -\frac{1}{2\mu}\Delta^2 + V(r). \tag{3.8}$$

The potential $V(r)$ could be Coulumbic $-\frac{1}{r}$, or Hartree-Fock type contains non-local exchange terms. The minimization requires

$$\frac{\partial}{\partial a^*(i,\lambda)}(<\chi_\lambda(\mathbf{r})|(H-E_\lambda)|\chi_\lambda(\mathbf{r})>) = 0. \tag{3.9}$$

This can be shown leads to the following matrix equation:

$$\mathbf{Ha} = E_\lambda \mathbf{Na}. \tag{3.10}$$

Here **H** is the Hamiltonian in the $\zeta$ representation and **N** is the identity matrix.

The basis states prepared with the above procedure are normalized to unity:

$$<\chi_\lambda(\mathbf{r})|\chi_\lambda(\mathbf{r})>= 1, \tag{3.11}$$

and they are orthogonal to each other:

$$<\chi_\lambda(\mathbf{r})|\chi_\lambda(\mathbf{r})'>= 0 \quad (\lambda \neq \lambda'). \tag{3.12}$$

This orthonormal requirement is important to the numerical stability of an FHBS calculation. For the basis states we prepared, the error is usually less than $10^{-10}$.

Typically after diagonization, for a particular angular momentum $l$, there are 3-6 bound states and 10-14 positive eigen-energy states in a basis. The bound states include those lowest energies states such as $|1s>, |2s>, |2p>$, etc. Those states played an important role in the ionization and charge-transfer in the collision and should be well represented.

We keep enough energy density for the pseudo-states, or discrete positive energy states, so we can interpolate to other energies without difficulty. However there is no need to keep very high energy states in our basis, since as a function of final state energy $E$, the cross section falls off approximately as $e^{-E}$. The highest positive energy state we keep is about 8 *au*. Our calculation shows the cross section has already fallen off more than two orders of magnitude at 8 *au* than it is at around 0 *au*.

The *Thomas mechanism* [19] is also reflected in the preparation of the basis. In the classical picture of the Thomas mechanism, the target electron is first scattered by the projectile proton at 60°. This electron is then scattered by the target proton and moving at the same speed as the projectile along the same direction. Since their relative speed is zero, the interaction time between projectile and electron would be longer than usual. This leads to larger electron capture by the projectile (charge transfer). To describe this mechanism, in the diagonized FHBS basis, there is always a state vector at the resonance energy of $v_p^2/2$, where $v_p$ is the speed of the projectile.

After we have prepared a reasonably satisfactory basis, a three-dimensional state with energy $E_\lambda$, angular momentum $l$,and $m$ is constructed from those radial basis states as

$$\chi_{\lambda,l}(r)y_{l,m}(\hat{\mathbf{r}}). \tag{3.13}$$

If the system starts at $1s$ state $|\Phi_0(t=0)>=|0>$, the system will evolve as

$$|\chi_0(t)>=\sum_{\lambda,l,m} U_{\lambda,l,m;0}(t)\chi_{\lambda,l}(r)y_{l,m}(\hat{\mathbf{r}}). \tag{3.14}$$

Here $U_{\lambda,l,m;0}(t)$ is the U-matrix transition element from the $1s$ state to $|\lambda,l,m>$, a state with energy $E_\lambda$ and angular momentum of $l$ and $m$. The U-matrix element is obtained by solving the time-dependent Schrödinger equation using SCE, OHCE, or TCE method.

The state basis in linear exponentials above could well describe the hydrogen system.

But by using the linear exponentials there are some difficulties when trying to evaluate certain integrals for the charge transfer matrix elements. Such integrals could be easily carried out if we are using Gaussian orbitals as

$$\zeta_i = r^l e^{-\alpha_i r^2} y_{l,m}(\hat{\mathbf{r}}). \tag{3.15}$$

However trying to use Gaussian orbitals directly diagonanized from the target or projectile Hamiltonian proved to be less numerically stable. The solution is to translate a well-diagonanized linear exponential basis into a Gaussian orbitals basis through a least-mean square fit. The translated Gaussian basis is used in the charge-transfer matrix element calculation. Other than the charge-transfer matrix integrals, the linear exponentials basis is used.

The state wave functions $|\chi_{\lambda,l}>$'s obtained from the above diagonization process are all normalized to unity. It is true regardless of whether the state is a bound state or scattering positive energy eigen-state. This is different from the real eigen-states of the Hamiltonian, where only bound states are normalized to unity. The real positive energy eigen-states, $|\chi(E_{\lambda,l})>$'s, are normalized to a boundary condition of unitary incoming flux. Define the projection operator **P** as

$$\mathbf{P} \equiv \sum_{\lambda,l,m} |\chi_{\lambda,l} y_{l,m}(\hat{\mathbf{r}}) >< \chi_{\lambda,l} y_{l,m}(\hat{\mathbf{r}})|, \tag{3.16}$$

where the index of $\lambda$ runs over the bound state and positive state. In the following for simplicity in discussion we ignore the angular momentum index $l$ and $m$ part and write our projection operator **P** as

$$\mathbf{P} \equiv \sum_{\lambda} |\chi_\lambda >< \chi_\lambda|. \tag{3.17}$$

Both the kinetic energy part and potential part of a target or projectile Hamiltonian are

projected onto our Hilbert space. The projection of potential part is

$$\mathbf{P}V\mathbf{P} = \sum_{\lambda}\sum_{\lambda'} |\chi_\lambda >< \chi_\lambda|V|\chi_{\lambda'} >< \chi_{\lambda'}|. \tag{3.18}$$

If the potential is a Coulomb potential, this projection leads to an effective finite range potential. To understand this observe the matrix element $< \chi_\lambda | -\frac{1}{r}|\chi_{\lambda'} >$ in the projection. The effective range of the Coulomb potential has been limited by the short range nature of $|\chi_\lambda >$. Hence there are only a finite number of negative energy states, or bound states, in our basis, as opposed to an infinite number of Rydberg states in the hydrogen system. The finite range of the potential enables us to calculate the phase in the wave function, which is essential in carrying out the differential cross sections in the TCE model. More on this in Chapter IV.

The projection onto the Hilbert basis of the kinetic energy discretized the continuum states and replaced them with a set of positive energy states, or pseudo-states. It is this discretization that makes the coupled channel method possible. However, in order to obtain a continuous and smooth differential cross section, we need to establish a connection between the continuum states and discretized pseudo-states. This connection is explained below.

The space constructed by the real eigen-functions and the pseudo-states are connected by the projection operator. Consider the sum

$$\sum_b |\chi_b >< \chi_b| + \int dE\rho(E)|\chi(E) >< \chi(E)| \tag{3.19}$$

where $|\chi_b >$'s are bound states and $|\chi(E) >$'s are positive energy states. $\rho(E)$ is a density function to be determined by normalization, which will be discussed later in this section.

Project this sum into the **P** space gives

$$\sum_b \mathbf{P}|\chi_b><\chi_b|\mathbf{P} + \int dE\rho(E)\mathbf{P}|\chi(E)><\chi(E)|\mathbf{P} = \mathbf{P}. \tag{3.20}$$

Replace the integral over $dE$ by a weighted sum with abscissas at pseudo state energies $\varepsilon_\lambda$, as we did in the Gaussian integration scheme, we will have

$$\sum_b \mathbf{P}|\chi_b><\chi_b|\mathbf{P} + \sum_\lambda \Delta_\lambda\ \rho(\varepsilon_\lambda)\mathbf{P}|\chi(\varepsilon_\lambda)><\chi(\varepsilon_\lambda)|\mathbf{P} = \mathbf{P}. \tag{3.21}$$

Here $\Delta_\lambda$ is the *weight* at abscissa energy $\varepsilon_\lambda$. We then approximate

$$\mathbf{P}|\chi(\varepsilon_\lambda)> = N_\lambda|\chi_\lambda>. \tag{3.22}$$

From Eq. (3.21) we obtain

$$|N_\lambda|^2\rho(\varepsilon_\lambda)\Delta_\lambda = 1. \tag{3.23}$$

The $\Delta_\lambda$'s and the abscissa energy $\varepsilon_\lambda$'s satisfy the *touching relationship*, as inferred from the integration scheme:

$$\varepsilon_{\lambda+1} - \varepsilon_\lambda = \Delta_{\lambda+1} - \Delta_\lambda. \tag{3.24}$$

If we can calculate $N_\lambda$, we can deduce $\Delta_\lambda$ from Eq. (3.23), and hence check those values against the touching relationship. We can them improve our basis set if it doesn't satisfy the touching relationship to a certain accuracy. Typically we think within 10% is acceptable, but we can relax our criterion for the last couple of energy states in our basis, where the scattering amplitude is small.

In the hydrogen system, since the exact wave function is known, the $N_\lambda$ can be calculated from Eq. 3.22. This is true to all atomic systems with known wave functions. But in a general many-electron atom system where the Hartree-Fock model is necessary, the

wave function is usually not known. The direct integral approach does not apply in such circumstance. A method of calculating $N_\lambda$ for unknown wave functions in a Hartree-Fock model is given in the next chapter.

Another less accurate method to calculate $N_\lambda$ in the case of unknown wave functions is to assume the integral starts from 0 for the first positive state energy $\varepsilon_1$. The weight is $\Delta_1$ for this energy. We can approximate

$$\Delta_1 = 2\varepsilon_1. \tag{3.25}$$

Then we can use the touching relationship to deduce all the $\Delta$'s, which in turn can be used to obtain the value of $N_\lambda$'s. For the Coulomb potential, this method is less satisfactory. The Rydberg states of the hydrogen system doesn't go to zero; they overlap with the positive energy states, so the value of $\Delta_1$ is not accurate enough to begin with the calculation. In any case if we use this method then we don't have an independent way to check the accuracy of the $N_\lambda$'s.

Lastly we need to establish the density function $\rho(\varepsilon_i)$ in Eq. (3.21) for the hydrogen system. For a unitary flux, the *l*th partial wave function with momentum of $\mathbf{k}$ is given by

$$|\mathbf{k}>_l = R_l(r)P_l(cos(\theta)). \tag{3.26}$$

Here $\theta$ is the angle formed by momentum vector $\mathbf{k}$ and position vector $\mathbf{r}$. By using the connection of Legendre polynomial $P_l(cos(\theta))$ to the spherical Harmonic $Y_{l,m}(\theta,\phi)$,

$$P_l(cos(\theta)) \;=\; \left(\frac{4\pi}{2l+1}\right)^{1/2} Y_{l,0}(\theta), \tag{3.27}$$

and the addition theorem of spherical harmonics,

$$\left(\frac{2l+1}{4\pi}\right)^{1/2} Y_{l,0}(\alpha) = \sum_{m=-l}^{l} Y^*_{l,m}(\theta,\phi)Y_{l,m}(\theta',\phi'), \tag{3.28}$$

this partial wave function can be expressed as

$$|\mathbf{k}>_l = R_l(r)\frac{4\pi}{2l+1}\sum_{m=0}^{l}[y^*_{l,m}(\hat{\mathbf{r}})y_{l,m}(\hat{\mathbf{k}}) - \bar{y}^*_{l,m}(\hat{\mathbf{r}})\bar{y}_{l,m}(\hat{\mathbf{k}})]. \tag{3.29}$$

From the approximation equation (3.22) we get

$$\mathbf{P}|\mathbf{k}>=\sum_l\sum_{m=0}^{l}\frac{4\pi}{2l+1}N_{\lambda,l}y_{l,m}(\hat{\mathbf{k}})\left|\chi_{\lambda,l}(r)y_{l,m}(\hat{\mathbf{r}})\right\rangle, \tag{3.30}$$

thus the integral

$$\begin{aligned}\int \mathbf{P}|\mathbf{k}><\mathbf{k}|\mathbf{P}\frac{d^3\mathbf{k}}{(2\pi)^3} &= \int\sum_{l'}\sum_{m'=0}^{l'}\frac{4\pi}{2l'+1}N_{\lambda',l'}y_{l',m'}(\hat{\mathbf{k}})\left|\chi_{\lambda',l'}(r)y_{l',m'}(\hat{\mathbf{r}})\right\rangle \\ &\quad \sum_l\sum_{m=0}^{l}\frac{4\pi}{2l+1}N^*_{\lambda,l}y^*_{l,m}(\hat{\mathbf{k}})\left\langle\chi_{\lambda,l}(r)y_{l,m}(\hat{\mathbf{r}})\right|\frac{d^3\mathbf{k}}{(2\pi)^3}. \end{aligned}\tag{3.31}$$

The expression above is simplified after integration over $d\Omega_{\vec{k}}$. The result is

$$\begin{aligned}&\int \mathbf{P}|\mathbf{k}><\mathbf{k}|\mathbf{P}\frac{d^3\mathbf{k}}{(2\pi)^3} \\ &= \int |N_{\lambda,l}|^2\frac{k^2dk}{(2\pi)^3}\sum_l\sum_{m=0}^{l}\left(\frac{4\pi}{2l+1}\right)^2\left|y_{l,m}(\hat{\mathbf{r}})\chi_{\lambda',l'}(r)\right\rangle\left\langle y_{l,m}(\hat{\mathbf{r}})\chi_{\lambda,l}(r)\right|. \end{aligned}\tag{3.32}$$

By comparing this sum with Eq. (3.21) we conclude that

$$\rho(E_\lambda) = \left(\frac{4\pi}{2l+1}\right)^2\frac{k_\lambda}{(2\pi)^3} = \frac{2/\pi}{(2l+1)^2}\sqrt{2E_\lambda}\ . \tag{3.33}$$

Eq. (3.33) is the expression used in the integration over the scattered electron energy $E_\lambda$.

## C. Single Centered Expansion

In general the Hamiltonian for a dynamic ion-atom collision system can be written as

$$H = H_t + V_p, \tag{3.34}$$

where $H_t$ is the target Hamiltonian. $V_p$ is the interaction between the projectile ion with charge $Z_p$ and the target electron. Assuming $\mathbf{r}$ is the vector from target center to the electron, and $\mathbf{R}(\mathbf{t})$ is the changing vector from target to the moving projectile position, then

$$V_p(\mathbf{r},\mathbf{R}(t),t) = \frac{-Z_p}{|\mathbf{R}(t)-\mathbf{r}|}, \tag{3.35}$$

and the Hamiltonian should be

$$H = -\frac{1}{2\mu}\nabla^2 - \frac{Z_t}{|\mathbf{r}|} - \frac{Z_p}{|\mathbf{R}-\mathbf{r}|}, \qquad \mathbf{R} = (\mathbf{B},\mathbf{v}t). \tag{3.36}$$

The electron's wave function must satisfy the time-dependent Schrödinger equation

$$i\frac{\partial}{\partial t}\Psi(t,t_0) = H\Psi(t,t_0). \tag{3.37}$$

The difference between SCE, OHCE, and TCE is on which basis set the electron wave function is expanded. In a SCE target-centered calculation, the wave function is expanded on a basis set, $\chi_\lambda(\mathbf{r})$'s, around the target, as

$$\Psi(t,t_0) = \sum_\lambda C_\lambda(t)\chi_\lambda(\mathbf{r})e^{-iE_\lambda t}. \tag{3.38}$$

Here $\chi_\lambda(\mathbf{r})$'s are eigen-states of target Hamiltonian $H_t$.

The substitution of the system's wave function into the time-dependent Schrödinger equation (3.37) leads to

$$i\frac{\partial}{\partial t}C_\lambda(t) = \sum_{\lambda'} V_{\lambda,\lambda'}e^{i(E_\lambda - E_{\lambda'})t}C_{\lambda'}(t), \tag{3.39}$$

where $V_{\lambda,\lambda'}$ is the matrix element. It is defined as

$$V_{\lambda,\lambda'} = < \chi_\lambda(\mathbf{r})|V_p(\mathbf{r},\mathbf{R}(t))|\chi_{\lambda'}(\mathbf{r}) > . \tag{3.40}$$

Further, if we consolidate the exponential energy factor into the matrix element $V_{\lambda,\lambda'}$ as

$$V'_{\lambda,\lambda'} = V_{\lambda,\lambda'} e^{i(E_\lambda - E_{\lambda'})t}, \tag{3.41}$$

and use the **U** matrix notation

$$\mathbf{C}(t) = \mathbf{U}(\mathbf{t}, \mathbf{t_0})\ \mathbf{C}(t_0), \tag{3.42}$$

then we can derive

$$i\frac{\partial}{\partial t}\mathbf{U}(t,t_0) = \mathbf{V}'\ \mathbf{U}(t,t_0). \tag{3.43}$$

With the transformation $Z = v_p t$ this gives the final expression used for numerical programming:

$$iv_p\frac{\partial}{\partial Z}\mathbf{U}(Z,Z_0) = \mathbf{V}'(\mathbf{B},Z)\ \mathbf{U}(Z,Z_0). \tag{3.44}$$

The first step in solving Eq. (3.44) is to calculate the matrix element, $V_{\lambda,\lambda'}$,

$$V_{\lambda,\lambda'} = -Z_p \int \chi^*_\lambda(\mathbf{r})\frac{1}{|\mathbf{R}(t)-\mathbf{r}|}\chi_{\lambda'}(\mathbf{r})\ d\mathbf{r}. \tag{3.45}$$

This integral can be simplified by separation of radial and angular parts. The idea is to expand the potential, $\frac{1}{|\mathbf{R}(t)-\mathbf{r}|}$, into a sum over radial and angular parts by using the addition theorem. However evaluation of each separated integral is still not trivial. Detailed evaluations and computer implementations of these integrals can be found in Dr. Martir's dissertation [20]. Once the matrix element $V_{\lambda,\lambda'}$ is calculated, the **U** matrix is obtained through a numerical integration over $Z$.

The SCE is the simplest method in FHBS theory family, and formed the basis for other FHBS methods. It has been proved to be useful in many areas. As noted, the disadvantage of the SCE is it is unable to effectively calculate the charge transfer between the target and the projectile. The is because a basis set centered around the target is difficult to describe

the wave functions around the projectile. Theoretically this is possible to describe any wave function in a complete basis set. But to achieve this in SCE requires increasing the basis to include unlimited number of states. A far better and effective way is to use either the OHCE or the TCE method.

## D. Two Centered Expansion

The Two Centered Expansion (TCE) method solved the difficulty of SCE by using two-basis set to describe the collision system: one basis set around the target and one around the projectile. In TCE, a system wave function $\Psi^{TCE}(t,t_0)$ can be expanded in this two-basis set as

$$\Psi^{TCE}(t,t_0) = \sum_{\lambda} C_{\lambda}^{T}(t)\chi_{\lambda}^{T}(\mathbf{r})e^{-iE_{\lambda}t} + \sum_{\lambda} C_{\lambda}^{P}(t)\chi_{\lambda}^{P}(\mathbf{r}-\mathbf{R})e^{-i\frac{v_P^2}{2}t}e^{i\mathbf{v_p}\cdot\mathbf{r}}e^{-iE_{\lambda}t}. \tag{3.46}$$

Here $\chi_{\lambda}^{T}(\mathbf{r})$ and $\chi_{\lambda}^{P}(\mathbf{r}-\mathbf{R})$ are target and projectile centered basis states; each satisfies its respective Hamiltonian equation.

The whole system evolves according to the same time-dependent Schrödinger equation as Eq. (3.37). In the integral form we have

$$\Psi_l^{TCE}(t,t_0) = \Psi_l^{SCE}(t,t_0) + i\sum \Psi_{l'}^{TCE}(t,t_0)\int_{t_0}^{t} \Psi_{l'}^{TCE}(t',t_0)(i\frac{\partial}{\partial t} - H)\Psi_l^{SCE}(t',t_0)dt'. \tag{3.47}$$

Or it can be expressed in the matrix formulation as

$$\Psi^{TCE}(t,t_0) = \Psi^{SCE}(t,t_0) + \Psi^{TCE}(t,t_0)\mathbf{O^{-1}}(\mathbf{t_0})\mathbf{A}(t,t_0). \tag{3.48}$$

Here the matrix element of **A** is defined as

$$A_{l',l}^{(+)} = i\int_{-\infty}^{t} \Psi_{l'}^{TCE}(t',-\infty)(i\frac{\partial}{\partial t} - H)\Psi_l^{SCE}(t',-\infty)dt'. \tag{3.49}$$

The matrix **O** is referred to as the overlap matrix. It is defined as

$$\mathbf{O}_{l',l}(t) = < \Psi_{l'} | \Psi_l > . \tag{3.50}$$

Let **E** be the identity matrix. the solution to Eq. (3.48) should be

$$\Psi^{TCE}(t,t_0) = \Psi^{SCE}(t,t_0) \frac{1}{\mathbf{E} - \mathbf{O}^{-1}(t_0)\mathbf{A}(t,t_0)}. \tag{3.51}$$

Thus the TCE can be calculated from the SCE and through proper integration. For detailed documentation see [21]. Most of the TCE computer program implementations were done by Mathew Fitzpatrick, while incorporated legacy programs contribution by others.

One disadvantage of the TCE over SCE or OHCE method is the numerical calculation is very slow. A production run of a TCE calculation will take about two months on our state-of-art Compaq Alpha UNIX system. Several other methods have been attempted to speed up the calculation but retain the merit and accuracy of TCE method, such as E-A theory described in [22] by Dr. Smith. But the approximations made by E-A theory made it not accurate enough to obtain differential cross sections at $20keV$ impact energy for a $p+H$ collision.

## E. One-and-Half-Centered-Expansion (OHCE)

The One-and-Half-Centered-Expansion (OHCE) is the same as the TCE, except there are no continuum states centered around the projectile. Compared to SCE, OHCE preserves TCE's ability to calculate the charge transfer between the target and projectile, which is considered important when interactions are strong. The inter-object ionization channel is omitted, however. Whether this omission will effect the differential cross section result is subject to numerical experimentation.

The advantage of using the OHCE method is it is simple to calculate the doubly dif-

ferential cross sections. In this method, the total differential cross sections are easily accounted for since the ionization is target-centered only. Applying OHCE method to calculate the $p+H$ ionized electron energy distribution at $48keV$ impact energy is successful, as shown in our previous work [4].

## F. Charge Transfer In the $p+H$ Collision

The inter-object charge transfer, such as the target electron captured by the projectile proton and being carried away as a bound state of the projectile, is an important subject in $p+H$ collisions. Though charge transfer is not the focus of this dissertation study, the accuracy of charge transfer cross sections from the TCE frame work is important to us, since the matrix elements are calculated by the same method and sharing the same computer code. A convincing charge transfer calculation could enhance our confidence in the doubly differential cross section results. Unfortunately it is difficult to experimentally measure the charge transfer possibility, so in most cases directly comparing with experimental results is not possible. The only reference is to compare with other theoretical results.

In his dissertation [21] Mathew Fitzpatrick used the FHBS TCE method to calculate $p+H$ K-shell and L-shell intra (excitation) and inter-object (charge transfer) for $50keV$, $75keV$, $100keV$ and $145keV$ impact energies. The comparison to other theories, CTMC and CDW, varies. Almost all theories agree on the $1s \rightarrow 1s$ state transition, but differ greatly on others. The difference for $s \rightarrow p$ or $p \rightarrow p$ type transition could be as high as 50% between different theories. Possible explanation of the difference might be due to the dipole nature of $p$ state. It is known transitions involving $p$ state occurs at a long distance in the p+H collision; convergence in distance can easily go awry if not treated properly.

Table III lists a $50keV$ impact energy charge transfer calculation including s-g and s-h partial waves using the FHBS TCE method, and compared to the CDW result. The FHBS

Table III. Comparison of Charge Transfer Calculation for $p+H$ Collision at $50keV$ Impact Energy

| | CDW ($10^{-17}$cm$^2$) | FHBS-g/cdw | FHBS-h/cdw |
|---|---|---|---|
| $1s-1s$ | 6.9500 | 0.999 | 0.991 |
| $1s-2s$ | 1.4400 | 0.972 | 0.979 |
| $1s-2p_0$ | 0.3950 | 0.516 | 0.509 |
| $1s-2p_1$ | 0.0872 | 0.931 | 0.933 |
| $2s-2s$ | 0.4450 | 1.371 | 1.373 |
| $2s-2p_0$ | 0.2630 | 0.779 | 0.791 |
| $2s-2p_1$ | 0.0357 | 1.860 | 1.787 |
| $2p_0-2p_0$ | 0.2200 | 0.450 | 0.403 |
| $2p_0-2p_1$ | 0.0363 | 1.680 | 1.645 |
| $2p_1-2p_1$ | 0.0150 | 2.487 | 2.620 |
| $2p_{+1}-2p_{-1}$ | 0.0411 | 1.187 | 1.280 |

result quoted here is using the same program as [21], but used a different integration scheme in the calculation of $U$ transition matrix. The results shown here also used a different basis. They only differ slightly from those the results given in [21].

## G. Obtaining the Angular and Energy Distribution

In the above sections we described the FHBS calculation of the transition matrix. In the following we will demonstrate how it is possible to obtain the differential cross sections from the information of $U$-matrix. Assuming at $t=-\infty$ the initial state of the electron is at

$\chi_0$, at time $t$ the dynamic wave function $\Phi_0^{(FHBS)}(t)$ should be

$$\Phi_0^{(FHBS)}(t) = \sum_{\lambda} e^{-i\varepsilon_\lambda t}\chi_\lambda \cdot U_{\lambda,o}(t,-\infty). \tag{3.52}$$

Here the U matrix $U_{\lambda,o}(\infty,-\infty)$ is obtained by solving the time-dependent Schrödinger equation, either in SCE, TCE or other FHBS theories. It satisfies

$$U_{\lambda,0}(\infty,-\infty) = \delta_{\lambda,0} - i\int \mathrm{d}t\ e^{i\varepsilon_\lambda t} < (H_t + V_p - \varepsilon_\lambda)\chi_\lambda \mid \phi_0^{(FHBS)} > . \tag{3.53}$$

The exact scattering amplitude is given by

$$T_0(E_\lambda) = -i\int \mathrm{d}t\ e^{iE_\lambda t} < (H_t + V_p - E_\lambda)\chi(E_\lambda) \mid \phi_0^{(+)} > . \tag{3.54}$$

Note the difference in equation (3.53) and equation (3.54). The $\varepsilon_\lambda$ and $\chi_\lambda$ refer to pseudo eigen-energy and state, while $E_\lambda$ and $\chi(E_\lambda)$ are the exact solutions obtained from solving the time-dependent Schrödinger equation $H_t\chi(E_\lambda) = E_\lambda\chi(E_\lambda)$. If we approximate the exact wave function $\phi_0^{(+)}$ with the FHBS solution we obtain

$$T_0(E_\lambda) = N_{\lambda,l}U_{\lambda,0}(\infty,-\infty). \tag{3.55}$$

Thus the scattering amplitude can be obtained from the knowledge of $N_{\lambda,l}$ and FHBS calculation of the U-matrix $U_{\lambda,0}$. It is obvious that we can only do this at pseudo state energies ($\varepsilon_\lambda$). However if we have sufficiently dense packing energy of the pseudo states, we can smoothly interpolate values of $T$ to other energy of our interest.

In the rest of this section we are going to describe how to obtain the doubly differential cross section from the U matrix in each respective frame. For a given U matrix associated with a particular partial wave $l$, $m$, $U_{i,0}^{l,m}(+\infty,-\infty)$, the corresponding scattering amplitude is

$$T_0^{l,m}(E_\lambda) = (-1)^l N_{\lambda,l}U_{\lambda,0}^{l,m}(+\infty,-\infty)y_{l,m}(\theta,\phi). \tag{3.56}$$

The origin of the factor, $(-1)^l$, is the same as when we are calculating the partial wave Born form factor: we used $\chi^{(+)}_{-\mathbf{k}}(\mathbf{r})$ in the matrix element. Generally $E_\lambda$'s are not the same for different angular momentum states. To solve this problem, we can interpolate the value of $N_{\lambda,l} \cdot U^{l,m}_{\lambda,0}(+\infty,-\infty)$ for each $l,m$ to a set of commonly predefined energies for all $l,m$'s. For this we used a simple three-points interpolation over the energy of $E_\lambda$'s. Below we still keep the notation of $E_\lambda = k^2/2$, but keep in mind those $E_\lambda$'s are the same for all $l,m$'s. By summing over all the partial waves we have the total scattering amplitude, $T_0(E_\lambda,\Omega)$:

$$T_0(E_\lambda,\Omega) = \sum_{l,m} T_0^{l,m}(E_\lambda). \tag{3.57}$$

To calculate energy distribution from $T_0(E_\lambda,\Omega)$, simply integrate over $d\Omega$, as

$$\int |T_0(E_\lambda,\Omega)|^2 d\Omega. \tag{3.58}$$

Eq. (3.58) is what we used to calculate energy distribution for $48keV$ impact energy [4]. It requires two steps to obtain the angular distribution. First we integrate over $d\phi$, and define the result as $d(\theta,E_\lambda)$,

$$d(\theta,E_\lambda) = \int_0^{2\pi} |T_0(E_\lambda,\Omega)|^2 d\phi = \int_0^{2\pi} |\sum_{l,m} T_0^{l,m}(E_\lambda)|^2 d\phi. \tag{3.59}$$

The angular distribution is obtained by integration over energy $E_\lambda$:

$$\int d(\theta,E_\lambda) dE_\lambda, \tag{3.60}$$

which is what we used in the previous chapter to calculate the B1 FHBS angular distribution.

With the above theoretical framework, we are now ready to explore the angular distribution at $20keV$ projectile energy using different FHBS theories. The SCE method is certainly not a good candidate, for at $20keV$ charge transfer and electron flux loss are im-

portant. To correctly reflect electron capture, transfer, and flux loss, either the OHCE or the TCE method should be used. Given the difficulty and complexity of the TCE method when it comes to calculate the differential cross section, we tried an OHCE calculation first.

In Fig. 4 we plot our OHCE results for the angular distribution, as well as the experimental data for the $p+H$ system at 20keV impact energy. The results is compare to CDW, CTMC calculations. Apparently the OHCE method fails to give good agreement with experimental data, even if we take into account of the $5-10\%$ error we commonly believe to have in an FHBS calculation. Our result is lower at forward scattering angles and higher at backward angles. The other two theoretical methods also fail to some extent. Both are lower at the large angles while the CTMC calculation tends to be lower than the experimental data throughout.

The explanation for the failure of the OHCE method could be in the missing continuum channel in the projectile center. The ionized electrons are steered away by both the target and projectile. The OHCE only uses the target ionization channel, which might be not effectively reflect the role of the projectile in the ionization. To account for these two channels effectively, it is necessary to use a TCE calculation. However if we use a TCE calculation, the procedure above only gives us the distribution in target and projectile respectively. To compare with experimental data, the TCE scattering distribution should be expressed in the target center only. This is described in the next chapter.

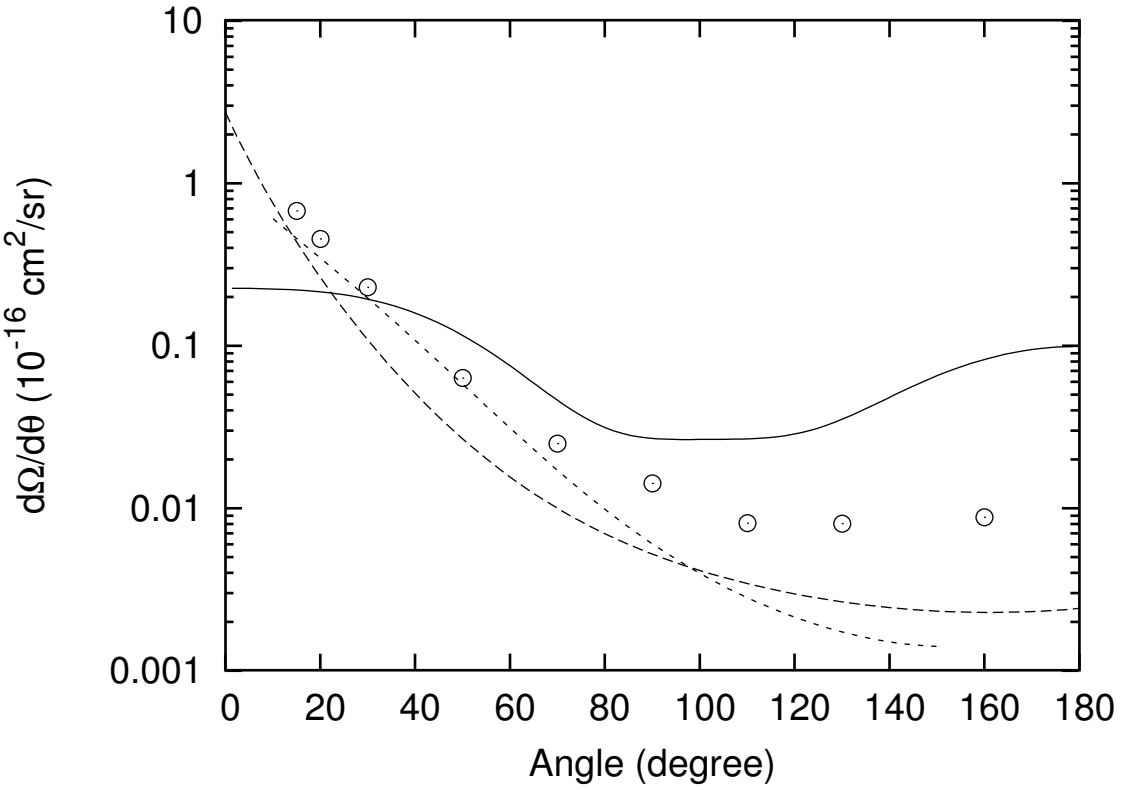


Fig. 4. Angular distribution of ionized electrons for at a $p+H$ collision at 20 keV impact energy given by OHCE, and compared to CDW, CTMC and experimental data. The theoretical results are: OHCE (solid line), CDW (dots), and CTMC (dotted line). The circled dots are experimental data.

# CHAPTER IV

# TWO-CENTERED FHBS METHOD

The failure of the OHCE method in re-producing the angular distribution shows the need to adopt the TCE method to effectively represent the electron flux loss through the projectile positive energy state channels. Using the procedure described in the previous chapter, we are able to calculate the scattering amplitudes at both centers in a TCE method: $T_0^T(E_\lambda, \Omega)$ for the target center and $T_0^P(E'_\lambda, \Omega')$ for the projectile center. The projectile centered amplitude, $T_0^P(E'_\lambda, \Omega')$, has to be translated into the target frame to be accounted for the total differential cross section. The angular momentum information in the the projectile scattered electron amplitude, $T_0^P(E'_\lambda, \Omega')$, makes this translation possible.

For a regular FHBS an electron is associated with the target center or the projectile center. The translated projectile amplitude describes the electron in the same momentum $\mathbf{k}$ as the target amplitude. The electron described by these two amplitudes is not distinguishable, and we need to consider the interference of these two amplitudes. In order to consider interference, the phase information of the electron wave function should be calculated. The approximation we made to connect a real wave function to our pseudo-state is Eq. (3.22), as

$$\mathbf{P}|\chi(\varepsilon_\lambda)>= N_{\lambda,l}|\chi_\lambda> .$$

The pseudo-state $|\chi_\lambda>$ is usually real and doesn't contain any phase information. All the phase information of the original wave function $|\chi(\varepsilon_\lambda)>$ is preserved in $N_{\lambda,l}$.

If we use a pure Coulomb field potential of the type $1/r$, retaining the wave function with accurate phase information is nearly impossible. This is due to the long range nature of the Coulomb potential. After a plane wave is being scattered from the Coulomb potential,

the electron wave function behaves asymptotically at large $r$ as

$$\chi_l \sim e^{\pm i(kr - n\ ln\ r)}. \tag{4.1}$$

Here $n = e^2/\hbar v$, where $v$ is the relative speed. The logarithmic contribution to the phase does not disappear as $r \to \infty$. It is difficult, if not impossible, to correctly represent this logarithmic phase in an FHBS calculation. A short-ranged potential should be used instead.

In this dissertation study a Hartree-Fock potential is used. In a Hartree-Fock potential the wave functions are localized, so there won't be a logarithmic-like phase contribution to the wave function as in Eq. (4.1). As pointed out in Chapter III, in the FHBS method we are using an effectively localized potential when we prepared a basis with the Coulomb potential. The projection of the potential into our Hilbert space limits its effective range.

## A. Calculating $N_{\lambda,l}$ in a Hartee-Fock Potential

This section aims to develop a method to calculate $N_{\lambda,l}$, which contains the phase information of the wave function. In the deduction we will use some asymptotic behavior of $j_l(kr)$ and $R_l(kr)$. The derivations follows the standard scattering theory.

Imaging an incoming flux of electrons being scattered by a potential $V$. Before scattering the electrons are described by the plane wave function, which in the partial wave expansion is

$$e^{i\mathbf{k}\cdot\mathbf{r}} = \sum_{l=0}^{\infty} i^l (2l+1) j_l(kr) P_l(\cos\theta). \tag{4.2}$$

The radial part of the expansion is Bessel function. At large distance ($r \to \infty$), the Bessel function $j_l(kr)$ behaves as

$$j_l(kr) \sim \frac{\cos(kr - \frac{1}{2}(l+1)\pi)}{kr}. \tag{4.3}$$

In the following discussion we need another similar function called *spherical Neumann function*. It is defined as

$$n_l(\rho) = (-1)^{l+1} \left(\frac{\pi}{2\rho}\right)^{\frac{1}{2}} J_{-l-\frac{1}{2}}(\rho) \tag{4.4}$$

At large distance ($r \to \infty$) the asymptotic expansion for $n_l(\rho)$ is

$$n_l(\rho) \sim \frac{1}{\rho} \cos[\rho - \frac{1}{2}(l+1)\pi] \tag{4.5}$$

Suppose after scattering, the electrons are in a state described by wave function $\Psi(\mathbf{r})$. In the partial wave expansion, the wave function $\Psi$ is

$$\Psi(\mathbf{r}) = \sum_{l=0}^{\infty} i^l (2l+1) \widetilde{R}_l(kr) P_l(\cos\theta). \tag{4.6}$$

Note the expansion above is slightly different from the expression used in Chapter II, in which case it is

$$\Psi(\mathbf{r}) = \sum_{l=0}^{\infty} R_l(kr) P_l(\cos\theta). \tag{4.7}$$

Obviously $R_l(kr) = i^l(2l+1)\widetilde{R}_l(kr)$. Some books use both expansion without distinguishing the difference between $R_l(kr)$ and $\widetilde{R}_l(kr)$, which might cause confusion.

It is known the general expression for $\widetilde{R}_l(kr)$ is

$$\widetilde{R}_l(kr) = e^{i\delta_l}[\cos\delta_l j_l(kr) - \sin\delta_l n_l(kr)]. \tag{4.8}$$

Here $\delta_l$ is a phase change caused by the presence of the potential $V$. After substituting the asymptotic form of the Bessel function and spherical Neumann function we obtain

$$\widetilde{R}_l(kr) \sim \frac{e^{i\delta_l} \sin(kr - \frac{1}{2}l\pi + \delta_l)}{kr}, \qquad (r \to \infty). \tag{4.9}$$

The function $j_l(kr)$ satisfies the following equation, which is taken from the radial part of the Schrödinger for the plane wave in the absence of potential $V$:

$$-\frac{1}{2}\frac{d^2}{dr^2}j_l(kr)-\frac{1}{r}\frac{d}{dr}j_l(kr)=\frac{1}{2}\left[k^2-\frac{l(l+1)}{r^2}\right]j_l(kr). \tag{4.10}$$

We can write a similar equation for $\widetilde{R}_l(kr)$:

$$-\frac{1}{2}\frac{d^2}{dr^2}\widetilde{R}_l(kr)-\frac{1}{r}\frac{d}{dr}\widetilde{R}_l(kr)+V\widetilde{R}_l(kr)=\frac{1}{2}\left[k^2-\frac{l(l+1)}{r^2}\right]\widetilde{R}_l(kr). \tag{4.11}$$

The difference between Eq. (4.10) and Eq. (4.11) is the second equation contains a potential term. The idea is to cross-multiply each equation by the other wave function in order to get rid of the duplicate terms, i.e. to perform

$$r^2[\widetilde{R}_l(kr)\times(4.10)-j_l(kr)\times(4.11)]$$

and then integrate distance $r$ over $(0,\infty)$. This gives

$$-\int_0^\infty dr\frac{d}{dr}[r^2W(\widetilde{R}_l(kr),j_l(kr))]=\int_0^\infty 2V(r)\widetilde{R}_l(kr)j_l(kr)r^2dr. \tag{4.12}$$

Here $W(\widetilde{R}_l(kr),j_l(kr))$ is known as the Wronskian; it is defined as

$$W(\widetilde{R}_l(kr),j_l(kr))=\widetilde{R}_l(kr)j_l'(kr)-\widetilde{R}_l'(kr)j_l(kr). \tag{4.13}$$

Using asymptotic equations for $j_l(kr)$ and $\widetilde{R}_l(kr)$, it can be shown that as $r\to\infty$,

$$\begin{aligned}
& r^2W(\widetilde{R}_l(kr),j_l(kr)) \\
= \;& e^{i\delta_l}r^2\left[\frac{\cos(kr-(l+1)\pi/2+\delta_l)}{kr}\cdot(-k)\frac{\sin(kr-(l+1)\pi/2)}{kr}\right. \\
& \left.+k\frac{\sin(kr-(l+1)\pi/2+\delta_l)}{kr}\frac{\cos(kr-(l+1)\pi/2)}{kr}\right] \\
= \;& e^{i\delta_l}\frac{\sin\delta_l}{k},
\end{aligned} \tag{4.14}$$

while as $r \to 0$, $r^2 W(\widetilde{R}_l(kr), j_l(kr)) \to 0$. This gives

$$-e^{i\delta_l} \sin\delta_l = k \int_0^\infty 2r^2 j_l(kr) V(r) \widetilde{R}_l(kr) dr. \tag{4.15}$$

Eq. (4.15) alone can not help us determine the phase since we don't know $\delta_l$. In search for a second equation, consider the wave function $\bar{z}_l(kr) = (1 - e^{-\beta r}) j_{l-1}(kr)$, where $\beta$ is small. Define a potential $\bar{V}$ that satisfies the following equation

$$-\frac{1}{2}\frac{d^2}{dr^2}\bar{z}_l(kr) - \frac{1}{r}\frac{d}{dr}\bar{z}_l(kr) = \frac{1}{2}\left[k^2 - \frac{l(l+1)}{r^2}\right]\bar{z}_l(kr) - \bar{V}\bar{z}_l(kr). \tag{4.16}$$

Note the above is only a definition equation. The potential $\bar{V}$ is not known to us, and it is to be determined later. Instead of $j_l(kr)$ we use $\bar{z}_l(kr)$ to repeat the same cross multiplication and subtraction procedure above with $\widetilde{R}_l(kr)$, i.e. to perform

$$r^2[\widetilde{R}_l(kr) \times (4.16) - \bar{z}_l(kr) \times (4.11)]$$

and integrate over $(0, \infty)$. This will eliminate some terms and we are left with

$$-\int_0^\infty dr \frac{d}{dr}[r^2 W(\widetilde{R}_l(kr), \bar{z}_l(kr))] = \int_0^\infty 2[V(r) - \bar{V}(r)]\widetilde{R}_l(kr)\bar{z}_l(kr) r^2 dr. \tag{4.17}$$

Again considering the asymptotic behavior of $\widetilde{R}_l(kr)$ and $j_l(kr)$ at large distance we have

$$\begin{aligned}
& r^2 W(\widetilde{R}_l(kr), \bar{z}_l(kr)) \\
= \;& e^{i\delta_l} r^2 \left[\frac{\cos(kr - (l+1)\pi/2 + \delta_l)}{kr} \cdot (-k) \frac{\sin(kr - l\pi/2)}{kr}\right. \\
& \left. + k \frac{\sin(kr - (l+1)\pi/2 + \delta_l)}{kr} \frac{\cos(kr - l\pi/2)}{kr}\right] \\
= \;& e^{i\delta_l} \frac{\sin(-\pi/2 + \delta_l)}{k} \\
= \;& -e^{i\delta_l} \frac{\cos\delta_l}{k}.
\end{aligned} \tag{4.18}$$

As usual as $r \to 0$ the Wronskian goes to zero. Thus we obtain the second equation,

$$e^{i\delta_l} \cos \delta_l = +k \int_0^\infty 2r^2 \widetilde{R}_l(kr)[V(r) - \bar{V}(r)]\bar{z}_l(kr)dr. \tag{4.19}$$

Eq. (4.19) together with Eq. (4.15) enables us to calculate the phase information in the electron wave function. First let's define

$$I_1 = \int_0^\infty r^2 \chi_l(kr) V(r) j_l(kr) dr, \tag{4.20}$$

$$I_2 = \int_0^\infty r^2 \chi_l(kr)[V(r) - \bar{V}(r)]\bar{z}_l(kr)dr. \tag{4.21}$$

Recall that we have made the assumption that $R_l(kr) = N_{\lambda,l}\chi_l(kr)$, where $\chi_l(kr)$ is our basis, and $R_l(kr) = i^l(2l+1)\widetilde{R}_l(kr)$. To simplify the expressions, define $\widetilde{N}_{\lambda,l}$ to satisfy

$$N_{\lambda,l} = i^l(2l+1)\widetilde{N}_{\lambda,l}. \tag{4.22}$$

This gives

$$\widetilde{R}_l(kr) = \widetilde{N}_{\lambda,l}\chi_l(kr). \tag{4.23}$$

Thus $(4.19) + i(4.15)$ gives

$$1 = 2k(I_2 + iI_1)\widetilde{N}_{\lambda,l}, \tag{4.24}$$

and the result for $N_{\lambda,l}$ is

$$N_{\lambda,l} = \frac{i^l(2l+1)}{2k(I_2 + iI_1)}. \tag{4.25}$$

If we can calculate $I_1$ and $I_2$ then $N_{\lambda,l}$ is easy determined. The detailed derivations of these two integrals are discussed in the next section.

B. Calculation of Integrals $I_1$ and $I_2$

In the following we define

$$\text{BESINT}(\alpha,k,l,DL) = \int_0^\infty e^{-\alpha r} r^{l+DL} j_l(kr) dr. \tag{4.26}$$

This definition refers to some frequently used integrals in this section. Here $\alpha$ is the exponential index in $e^{-\alpha r}$, while $l$ is the order of the Bessel function $j_l(kr)$ and $k$ is the coefficient. $DL$ is the difference between the power in $r$ and the order of the Bessel function. For example, if we are doing integral

$$\int_0^\infty e^{-\alpha r} r^3 j_1(kr) dr,$$

then $L = 1$ and $DL = 2$. For the integral (4.26) to have an analytical solution, the value of $DL$ should be either 1, 2 or 3. The results of these integrals are listed in Appendix A and are programmed into computer code.

In the following we can using a Yukawa potential, $V = -\frac{e^{-\gamma r}}{r}$. Here $\gamma$ is an indicator of the effective range of the potential. Calculations of $N_\lambda$ should be independent of our choice of $\gamma$. In the exponential basis $\chi_l(r) = \sum_i a_i e^{-\alpha_i r} r^l$. With these information, it is easy to work out the first integral $I_1$:

$$\begin{aligned} I_1 &= \int_0^\infty r^2 \chi_l(kr) V(r) j_l(kr) dr \\ &= -\sum_i a_i \int_0^\infty e^{-(\alpha_i+\gamma)r} r^{l+1} j_l(kr) dr \\ &= -\sum_i a_i \text{BESINT}(\alpha_i+\gamma,k,l,1). \end{aligned} \tag{4.27}$$

The second integral, $I_2$, has two parts. Each will be worked out separately. Define the

first part of $I_2$ which contains only the potential $V$ as

$$I_{21} = \int_0^\infty r^2 \chi_l(kr) V(r) \bar{z}_l(kr) dr. \tag{4.28}$$

Upon using the integral BESINT, the result is

$$\begin{aligned} I_{21} &= -\sum_i a_i \int_0^\infty [e^{-\alpha_i+\gamma r} - e^{-(\alpha_i+\gamma+\beta)r}] r^{l+1} j_{l-1}(kr) dr \\ &= -\sum_i a_i \big[ + \text{BESINT}(\alpha_i+\gamma, k, l-1, 2) \\ &\qquad -\text{BESINT}(\alpha_i+\gamma+\beta, k, l-1, 2)\big]. \end{aligned} \tag{4.29}$$

The second part in $I_2$ contains the potential $\bar{V}$, and we define this integral as

$$I_{22} = \int_0^\infty r^2 \chi_l(kr) \bar{V}(r) \bar{z}_l(kr) dr. \tag{4.30}$$

As mentioned in the previous section, we don't have an explicit expression for potential $\bar{V}$. To work out this integral, we substitute the whole term, $\bar{V}(r)\bar{z}_l(kr)$, into the integral by using the definition Eq. (4.16), as

$$I_{22} = \int_0^\infty r^2 \chi_l(kr) \cdot \left( \frac{1}{2}\frac{d^2}{dr^2} + \frac{1}{r}\frac{d}{dr} + \frac{1}{2}\left[ k^2 - \frac{l(l+1)}{r^2} \right] \right) \bar{z}_l(kr) dr. \tag{4.31}$$

There are two methods to finish this integral. One method is to directly differentiate $z_l(kr)$, which will generate many terms and incur several integrals. The details of this calculation have been documented in appendix B. An easier approach is to concentrate on the first two terms. It can be shown that

$$\int_0^\infty r^2 \chi_l(kr) \cdot \left[ \frac{1}{2}\frac{d^2}{dr^2} + \frac{1}{r}\frac{d}{dr} \right] \bar{z}_l(kr) dr = \frac{1}{2} \int_0^\infty \chi_l(kr) \cdot \frac{d}{dr} \left[ r^2 \frac{d\bar{z}_l(kr)}{dr} \right] dr. \tag{4.32}$$

The integral in Eq. (4.32) can be done by integrating by parts. Note the asymptotic behavior

of $\chi_l(kr)$ and $j_l(kr)$ near $r=0$ and $r\to\infty$, we have

$$\int_0^\infty \chi_l(kr)\cdot\frac{d}{dr}\left[r^2\frac{d\bar{z}_l(kr)}{dr}\right]dr=\int_0^\infty \bar{z}_l(kr)\cdot\frac{d}{dr}\left[r^2\frac{d\chi_l(kr)}{dr}\right]dr. \tag{4.33}$$

Since $(r^l e^{-\alpha_i r})'=(lr^{l-1}-\alpha r^l)e^{-\alpha_i r}$, $r^2(r^l e^{-\alpha_i r})'=(lr^{l+1}-\alpha r^{l+2})e^{-\alpha_i r}$, and

$$\frac{d}{dr}\left[r^2\frac{d(r^l e^{-\alpha_i r})}{dr}\right]=[\ l(l+1)r^l-\alpha_i(l+2)r^{l+1}-\alpha l r^{l+1}+\alpha^2 r^{l+2})]e^{-\alpha_i r}, \tag{4.34}$$

the contributions from the first two terms to the integral turn out to be

$$\frac{d}{dr}\left[r^2\frac{d\chi_l(kr)}{dr}\right]=\sum_i a_i\ [\ l(l+1)r^l-2\alpha_i(l+1)r^{l+1}+\alpha_i^2 r^{l+2}\ ]e^{-\alpha_i r}. \tag{4.35}$$

Combined with contributions from other terms, the result for the second integral is

$$\begin{aligned} I_{22}=\frac{1}{2}\sum_i a_i\Big[\ &+\ l(l+1)\int_0^\infty(1-e^{-\beta r})j_{l-1}(kr)r^l e^{-\alpha_i r}dr\\ &-\ 2\alpha_i(l+1)\int_0^\infty(1-e^{-\beta r})j_{l-1}(kr)r^{l+1}e^{-\alpha_i r}dr\\ &+\ \alpha_i^2\int_0^\infty(1-e^{-\beta r})j_{l-1}(kr)r^{l+2}e^{-\alpha_i r}dr\\ &+\ k^2\int_0^\infty(1-e^{-\beta r})j_{l-1}(kr)r^{l+2}e^{-\alpha_i r}dr\\ &-\ l(l+1)\int_0^\infty(1-e^{-\beta r})j_{l-1}(kr)r^l e^{-\alpha_i r}dr\ \Big]. \end{aligned} \tag{4.36}$$

The first and last term cancel. After grouping terms that have the same type of integrals, we have

$$\begin{aligned} I_{22}=\frac{1}{2}\sum a_i\Big[\ &-\ 2\alpha_i(l+1)\int_0^\infty(1-e^{-\beta r})j_{l-1}(kr)r^{l+1}e^{-\alpha_i r}dr\\ &+\ (\alpha_i^2+k^2)\int_0^\infty(1-e^{-\beta r})j_{l-1}(kr)r^{l+2}e^{-\alpha_i r}dr\ \Big]. \end{aligned} \tag{4.37}$$

Expressed in the BESINT notation the result is

$$I_{22} = \frac{1}{2}\sum a_i \Big\{ \quad - \quad 2\alpha_i(l+1)[\text{BESINT}(\alpha_i,k,l-1,2) - \text{BESINT}(\alpha_i+\beta,k,l-1,2)] \\ + \quad (\alpha_i^2+k^2)[\text{BESINT}(\alpha_i,k,l-1,3) - \text{BESINT}(\alpha_i+\beta,k,l-1,3)] \Big\}. \tag{4.38}$$

Thus we complete our derivation of all the integrals for $I_1$ and $I_2$, where $I_2 = I_{21} - I_{22}$. Once these values are obtained, $N_{\lambda,l}$ can be calculated by using Eq. (4.24) as

$$N_{\lambda,l} = \frac{i^l(2l+1)}{2k(I_{21} - I_{22} + iI_1)}. \tag{4.39}$$

Two checks have be proposed to check the accuracy of $N_l$, since the above procedure is complicated and involves lots of numerical programming. The first check is from observing Eq. (4.15),

$$-2kI_1\widetilde{N}_{\lambda,l} = e^{i\delta_l}\sin\delta_l.$$

If take modulus of both sides we have

$$|2kI_1\widetilde{N}_{\lambda,l}|^2 = \sin^2\delta_l. \tag{4.40}$$

On the other hand, taking the imaginary part of both sides of the equation leads to

$$Imag(-2kI_1\widetilde{N}_{\lambda,l}) = \sin^2\delta_l. \tag{4.41}$$

Thus we have a identity as our first check:

$$Imag(-2kI_1\widetilde{N}_{\lambda,l}) = |2kI_1\widetilde{N}_{\lambda,l}|^2, \tag{4.42}$$

The second check comes from Eq. (4.15) - i Eq. (4.19), which gives

$$-e^{i\delta_l}\cos\delta_l - ie^{i\delta_l}\sin\delta_l = 2k(I_2 - iI_1). \tag{4.43}$$

Taking modulus of both sides of the equation gives the second identity of our test:

$$|2k(I_2 - iI_1)\cdot\widetilde{N}_{\lambda,l}| = 1. \tag{4.44}$$

A successful calculation of $\widetilde{N}_{\lambda,l}$ should pass both two tests.

Table IV lists $N_{\lambda,l}$ values for $p(l=1)$ states of a basis prepared for a $p+H$ collision at $20keV$ impact energy. The values are for two different value of $\gamma$ in the Hartree-Fock potential. Over all we have 19 states, with 6 bound states and 13 positive energy states (pseudo-states). The values of $N_{\lambda,l}$ are unit for bound states by definition. The values of $N_{\lambda,l}$ for pseudo-states differ little for low energy states as the parameter $\gamma$ changes; at some high energy states the maximum percentage error is 20%. The difference at high energy states would barely affect our calculation if we note that the exponential drop of differential cross sections as a function of the final state energy $E$. Detailed FHBS calculation at $20keV$ impact energy shows at $E = 8\ au$ the cross sections drops at least two magnitude from those at around 0 $au$.

## C. Transformation of Projectile Amplitude

As described in the previous chapter, it is possible to obtain a scattering amplitude of momentum in the target center or projectile center from a TCE FHBS calculation. This scattering amplitude can be calculated from the $U$-matrix as

$$T_0(E_\lambda,\Omega) = \sum_{l,m}(-1)^l N_{\lambda,l}U^{l,m}_{\lambda,0}(+\infty,-\infty)y_{l,m}(\theta,\phi). \tag{4.45}$$

Table IV. Sample Values of $N_{\lambda,l}$ for $p$ ($l = 1$) States

| n | energy (a.u) | $N_{\lambda,l}(\beta = 0.5)$ | $N_{\lambda,l}$ $(\beta = 1.0)$ |
|---|---|---|---|
| 1 | -0.125 | (1.00, 0.00) | (1.00, 0.00) |
| 2 | -0.667 | (1.00, 0.00) | (1.00, 0.00) |
| 3 | -0.0322 | (1.00, 0.00) | (1.00, 0.00) |
| 4 | -0.0200 | (1.00, 0.00) | (1.00, 0.00) |
| 5 | -0.0137 | (1.00, 0.00) | (1.00, 0.00) |
| 6 | -0.007 | (1.00, 0.00) | (1.00, 0.00) |
| 7 | 0.006 | (-51.6, -41.1) | (-51.6, -41.1) |
| 8 | 0.0298 | (-9.02, 40.3) | (-9.01, 40.3) |
| 9 | 0.0704 | (-19.1, 19.2) | (-19.1, 19.2) |
| 10 | 0.136 | (-13.4, -10.8) | (-13.4, -10.8) |
| 11 | 0.240 | (11.3, -6.07) | (11.3, -6.06) |
| 12 | 0.400 | (-1.40, 8.91) | (-1.40, 8.90) |
| 13 | 0.644 | (-2.98, -5.54) | (-2.98, -5.54) |
| 14 | 1.01 | (3.80, 2.56) | (3.80, 2.56) |
| 15 | 1.56 | (-3.35, -0.721) | (-3.36, -0.702) |
| 16 | 2.38 | (2.59, -0.265) | (2.59, -0.290) |
| 17 | 3.58 | (-1.86, 0.663) | (-1.82, 0.711) |
| 18 | 5.35 | (1.31, -0.804) | (1.25, -0.833) |
| 19 | 7.87 | (-0.909, 0.722) | (-0.767, 0.741) |

In the following we use $T_0^T(E_\lambda,\Omega)$ and $T_0^P(E'_\lambda,\Omega')$ to refer to the target and projectile amplitude. Here $\Omega$ and $\Omega'$ are solid angles in each respective frame, and $E_\lambda = k^2/2$ and $E'_\lambda = k'^2/2$, where $k$ and $k'$ are momentum magnitude in the target and projectile center.

The projectile contribution, $T_0^P(E'_\lambda,\Omega')$, needs to be transformed to the target frame to add up with the target contribution. Let $\mathbf{k}$ be the momentum in the target frame, $\mathbf{v_p}$ be projectile velocity, and $\mathbf{k}'$ be the momentum in the projectile frame, these three vectors satisfy

$$\mathbf{k} - \mathbf{v_p} = \mathbf{k}'. \tag{4.46}$$

Or in the magnitude and angle representation,

$$\begin{aligned} k^2 &= v_p^2 + k'^2 + 2\mathbf{k}'\cdot\mathbf{v_p} \\ \cos\theta &= \frac{k'\cos\theta' + v_p}{k}. \end{aligned} \tag{4.47}$$

Here $\theta$ is the angle formed by $\mathbf{k}$ and $\mathbf{v_p}$ while $\theta'$ is the angle formed by $\mathbf{k}'$ and $\mathbf{v_p}$. In our calculation the $\mathbf{v_p}$ direction is taken as $z$ axis. Using this Galilean transformation, the projectile amplitude $T_0^P(E'_\lambda,\Omega')$ can be translated into the target frame. We define the translated amplitude as $T_0^P(E_\lambda,\Omega)$.

However there is a practical problem. In the FHBS diagonalization, for a chosen target there are a set of eigen-energies for all $l$ such that

$$\frac{k^2}{2} = E_\lambda \tag{4.48}$$

while for the projectile there are a set of pseudo-states where the eigen-energies for all $l'$ as

$$\frac{|\mathbf{k}'|^2}{2} = \frac{|\mathbf{k}-\mathbf{v_p}|^2}{2} = E_{\lambda'}. \tag{4.49}$$

For an arbitrary $\mathbf{k}$ usually it is hard to find a pair of states in the target and projectile pseudo-states whose eigen-energies would satisfy both conditions. The solution is to reverse the

transformation, i.e., given a momentum $\mathbf{k}$, find $\mathbf{k}'$ in the projectile frame. This means to write the pair Eq. (4.47) as

$$\begin{aligned} k'^2 &= k^2 - v_p^2 - 2\mathbf{k}\cdot\mathbf{v_p} \\ \cos\theta' &= \frac{k\cos\theta - v_p}{k'}, \end{aligned} \tag{4.50}$$

and then interpolate the quantity $N_{\lambda',l'}U^{l',m'}_{\lambda',0}(+\infty,-\infty)$ in the projectile frame. The same set of chosen $\mathbf{k}$'s are also used to interpolate the quantity $N_{\lambda,l}U^{l,m}_{\lambda,0}(+\infty,-\infty)$ which is the target frame. This way the two interpolated values from target and projectile are in a common set of energy and angle values, which can be used to obtain the differential cross sections of our interest.

## D. Interference

Our final ionized electron wave function [23]

$$\chi(\mathbf{k},\mathbf{r})e^{-ik^2t/2} = \chi_T^{(-)}(\mathbf{k},\mathbf{r})e^{-ik^2t/2} + e^{i\mathbf{v}\cdot\mathbf{r}+i\mathbf{k}\cdot\mathbf{B}}\chi_P^{(-)}(\mathbf{k}-\mathbf{v},\mathbf{r}-\mathbf{R})e^{-i(\mathbf{k}-\mathbf{v})^2t/2-ivZ/2} - e^{i\mathbf{k}\cdot\mathbf{r}-ik^2t/2} \tag{4.51}$$

As $t\to\infty$, in the target region only the first term survives. The second term, the contribution from the projectile, behaves as a plane wave which is the third term. In the projectile region it is a similar situation except it is the target term which cancels with the plane wave. This two contribution from the target and projectile pseudo-states projected into system amplitude would give us the angular and energy distribution.

After the transformation and interpolation we could easily add up the contribution to obtain angular and energy distribution. The projectile contribution $T_0^P(E_\lambda,\Omega)$ has an additional phase $e^{i\mathbf{k}\cdot\mathbf{B}}$ from the above argument. In order to obtain the angular contribution

we need to integrate over the angle $\phi_k$ as

$$\int |T_0^T(E_\lambda,\Omega) + e^{i\mathbf{k}\cdot\mathbf{B}} T_0^P(E_\lambda,\Omega)|^2 d\phi_k. \tag{4.52}$$

The difficulty in evaluating the above integral is in the cross terms. From the additional theorem we have

$$\cos(\hat{\mathbf{k}}\cdot\hat{\mathbf{B}}) = \cos\theta_k\cos\theta_B + \sin\theta_k\sin\theta_B\cos(\phi_k - \phi_B), \tag{4.53}$$

where $\theta_k$, $\theta_B$, $\phi_k$ and $\phi_B$ are angles formed with an arbitrary axis. Note the impact parameter vector $\mathbf{B}$ is perpendicular to the projectile velocity $\mathbf{v_p}$. If we take $\mathbf{v_p}$ as our $z$ axis and $\mathbf{B}$ as $x$ axis, then $\theta_B = \pi/2$ and $\phi_B = 0$. This leads to

$$\cos(\hat{\mathbf{k}}\cdot\hat{\mathbf{B}}) = \sin\theta_k\cos\phi_k. \tag{4.54}$$

Thus the first cross term is

$$T^*\cdot P\cdot e^{ikB\sin\theta_k\cos\phi_k}\frac{2\cos m\phi_k}{\sqrt{2(1+\delta_m,0)}}\frac{2\cos m'\phi_k}{\sqrt{2(1+\delta_{m'},0)}}. \tag{4.55}$$

Here $T$ and $P$ refer to the target and projectile contribution terms, but without the $\cos m\phi_k$ or $\cos m'\phi_k$ functions. The second cross term should be the complex conjugate of the first term.

Since

$$\cos m\phi_k\cos m'\phi_k = \frac{\cos(m-m')\phi_k + \cos(m+m')\phi_k}{2}, \tag{4.56}$$

we have

$$T^*\cdot P\cdot e^{ikB\sin\theta_k\cos\phi_k}\frac{\cos(m-m')\phi_k + \cos(m+m')\phi_k}{\sqrt{(1+\delta_m,0)}\sqrt{(1+\delta_{m'},0)}}. \tag{4.57}$$

So the first cross term integration over $\phi_k$ is

$$\frac{T^* \cdot P}{\sqrt{(1+\delta_m,0)}\sqrt{(1+\delta_{m'},0)}} \int_0^{2\pi} e^{ikB\sin\theta_k\cos\phi_k} \left[\cos(m-m')\phi_k + \cos(m+m')\phi_k\right] d\phi_k. \tag{4.58}$$

To evaluate this integral let's consider this property of the Bessel function (see 9.1.21 of [16]):

$$J_n(z) = \frac{i^{-n}}{\pi} \int_0^{\pi} e^{iz\cos\theta} \cos(n\theta) d\theta. \tag{4.59}$$

If we aware that $\cos n\theta$ is even within $[0, 2\pi]$ around $\pi$, we have

$$\int_0^{2\pi} e^{iz\cos\theta} \cos(n\theta) d\theta = \int_0^{2\pi} e^{iz\cos\theta} \cos(|n|\theta) d\theta, \tag{4.60}$$

and

$$\int_0^{2\pi} e^{iz\cos\theta} \cos(|n|\theta) d\theta = 2\int_0^{\pi} e^{iz\cos\theta} \cos(|n|\theta) d\theta. \tag{4.61}$$

This gives

$$\int_0^{2\pi} e^{iz\cos\theta} \cos(n\theta) d\theta = 2\pi \cdot i^{|n|} J_{|n|}(z). \tag{4.62}$$

Note in the above equation $n$ is replace by $|n|$. The $d\phi_k$ integration for the first cross terms gives

$$\frac{T^* \cdot P}{\sqrt{(1+\delta_m,0)}\sqrt{(1+\delta_{m'},0)}} \cdot \left[2\pi \cdot i^{(|m-m'|)} J_{(|m-m'|)}(kB\sin\theta_k) + 2\pi \cdot i^{(|m+m'|)} J_{(|m+m'|)}(kB\sin\theta_k)\right]. \tag{4.63}$$

The second cross term integrated over $d\phi_k$ should give the complex conjugate of the above expression. The total contribution from those two interference terms is twice the real part of Eq. (4.63).

## E. Results of Angular and Energy Distributions from TCE

In a TCE FHBS method, electrons are treated separately in each center. Transition probabilities are calculated and associated with each respective center. Electrons from each center are distinguishable. Total transition possibilities are obtained by adding up the two probabilities from target and projectile.

The translation of the projectile scattering amplitude enables us to describe the projectile electron in the same momentum **k** as the target electron. Electrons described by those two amplitudes are thus not distinguishable. This leads to the possible interference between the target amplitude $T_0^T(E_\lambda, \Omega)$ and translated projectile amplitude $T_0^P(E_\lambda, \Omega)$. However in practice we can still add up incoherently these two contribution as

$$|T_0^T(E_\lambda, \Omega)|^2 + |T_0^P(E_\lambda, \Omega)|^2. \tag{4.64}$$

From this we can explore the effect of the additional projectile continuum scattering channel added in the TCE over the OHCE method. In Fig. (5) we plotted out this incoherent TCE result for the angular distribution. The incoherent TCE is a big improvement over the OHCE. This suggests that at $20keV$, the additional projectile continuum channel is needed to improve the efficiency in steering away the electrons. As suggested by the comparison, under the influence of the projectile more electrons are ejected into the forward scattering angle.

The comparison of incoherent and coherent is interesting. In Fig. (5) and Fig. (6) we plot the angular and energy distribution with and without the interference effects. In both results, the additional interference term between the target and projectile amplitude helps the calculation to match experimental data. For the angular distribution the interference helps improves the calculation in the (20°, 100°) angle region; while in the energy distribution the interference bolsters the energy distribution at lower energies. The interference

doesn't solve our problems at higher angles for the angular distribution.

The interference effect might be explained by the following: during a $p+H$ collision the electron is being scattered by the target and projectile protons; the electron develops a phase difference when it travels two different paths from the two protons; this phase difference leads to the interference of the two amplitudes from each center. The fact that the projectile proton is always moving makes the interference a little subtle. This effect, absent in SCE and OHCE, represents a new aspect of the TCE in obtaining the differential cross section calculation during an ion-atom collision.

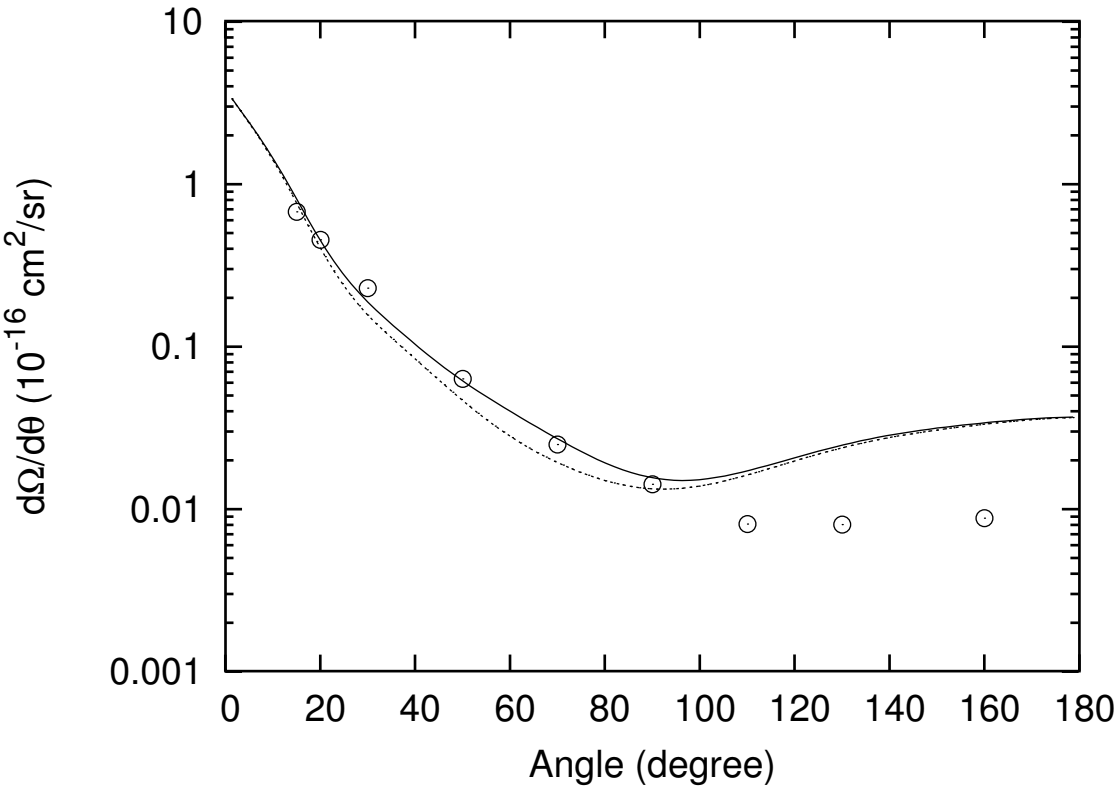


Fig. 5. Angular distribution of ionized electrons at 20 keV projectile energy $p+H$ collision given by Two-Centered-Expansion method. Results are TCE with interference (solid line) and without interference (dotted line). The circled dots are experimental data.

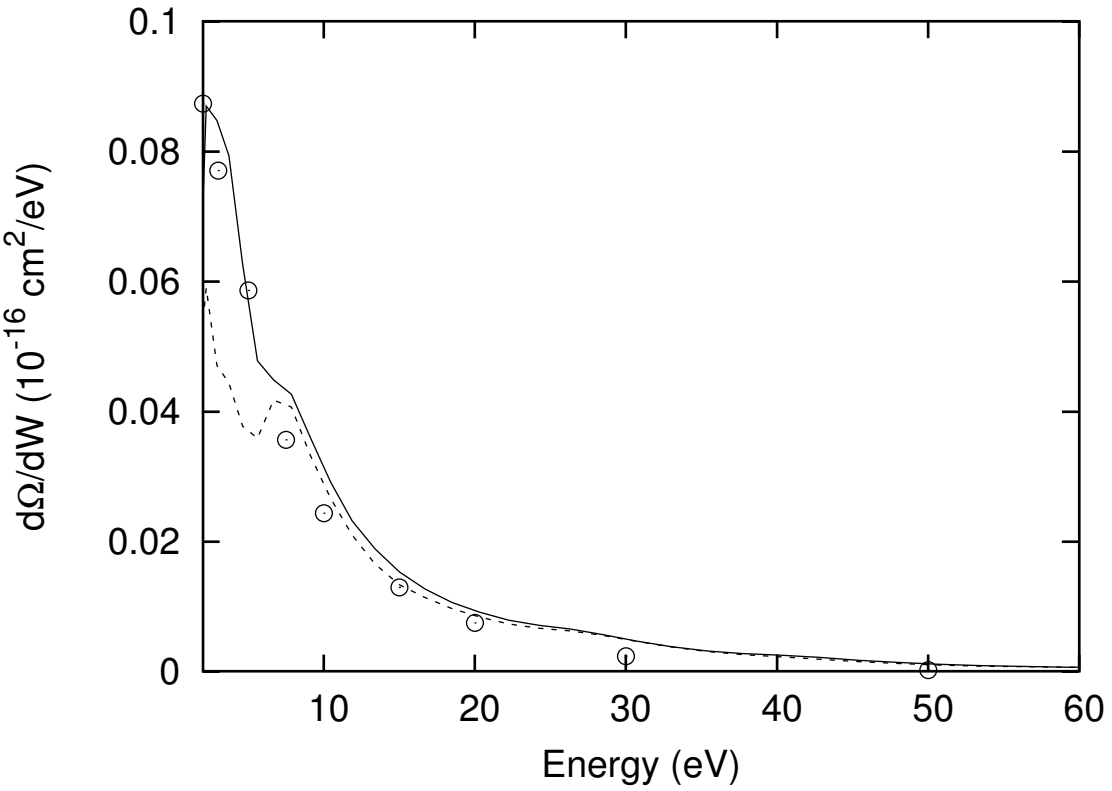


Fig. 6. Energy distribution of ionized electrons at 20 keV projectile energy $p+H$ collision given by Two-Centered-Expansion method. Results are TCE with interference (solid line) and without interference (dotted line). The circled dots are experimental data.

# CHAPTER V

# CONCLUSIONS

In this dissertation an FHBS method is developed to calculate the angular and energy distribution for ionized electrons in a ion-atom collision. This method is applied to the $p+H$ collision at $20keV$ impact energy. At this impact energy the interactions between the target proton, projectile proton and the electron are strong. The calculations shows a TCE FHBS method is necessary to include the charge transfer of electrons, and to effectively describe the steering away of electrons by the target and projectile protons. We discovered when we included the interference between two exit channels of projectile and target in the TCE calculation, our angular and energy distribution results agree reasonably well with experimental data. This interference effect is unexpected.

We still have the difficulty in giving satisfactory result at small differential cross sections. This failure could be from the cancellation of terms when adding up all the partial waves contributions. The error from FHBS calculation coupled with less-precise phase information might lead to the difference with experimental data. One possible fix is to improve the basis which will enable use to calculate the phase information more accurately.

The direct further work following this dissertation is to apply the FHBS calculation to the ion-atom collision. The method described in this dissertation uses a Hartree-Fock potential. There should be no intrinsic difficulty in applying this method to obtain differential cross sections for a ion-and-many-electron-atom collision. What is needed is a properly diagonized basis using a Hamiltonian with many-body potential, and to re-evaluate $N_{\lambda,l}$ in this new potential to keep phase information of the wave function. To compare with experiment, one might need to include the effects of secondary-ionized Auger electrons to the differential cross sections. This will helps us better understand the DNA breaking process by high speed protons mentioned in the introduction.

Another application of the method is to examine the existence of the *bus stop effect* [24, 25, 26]. This effect is a theoretical prediction that the proton cross section, $\sigma_+$ would be less than the Born cross section, $\sigma_B$, and the anti-proton cross section, $\sigma_-$, is greater than $\sigma_B$. Previous FHBS calculation [27] using the second order of scattering amplitudes with a Yukawa-type potential shows there is no such effect. It is hoped that a calculation using the current method will shed more light on this matter.

# REFERENCES

[1] M. A. Herve du Penhoat, B. Fayard, F. Able, A. Touati, F. Gobert, I. Despiney-Bailly, M. Ricoul, L. Sabateir, D. L. Stevens, M. A. Hill, D. T. Goodhead and A. Chetioui, Radiation Research **151**, 649 (1999).

[2] M. W. Gealy, G. W. Kerby III, Y. Y. Hsu and M. E. Rudd, Phys. Rev. A **51**, 2247 (1995).

[3] G. W. Kerby III, M. W. Gealy, Y. Y. Hsu, M. E. Rudd, D. R. Schultz and C. O. Reinhold, Phys. Rev. A **51**, 2256 (1995).

[4] J. Fu, M. J. Fitzpatrick, J. F. Reading and R. Gayet, J. Phys. B: At. Mol. Opt. Phys. **34**, 15 (2001).

[5] R. E. Olson and A. Salop, Phys. Rev. A **16**, 531 (1977).

[6] R. Abrines and I. C. Percival, Proc. Phys. Soc. Lond. **88**, 861 (1966).

[7] I. M. Cheshire, Proc. Phys. Soc. **84** 89 (1964)

[8] P. D. Fainstein, V. H. Ponce and R. D. Rivarola, J. Phys. B: At. Mol. Opt. Phys. **24**, 3091 (1991).

[9] E. Y. Sidky and C. D. Lin, J. Phys. B: At. Mol. Opt. Phys. **31**, 2949 (1998).

[10] A. Kolakowska, M. S. Pindzola, F. Robicheaux, D. R. Schultz, and J. C. Wells, Phys. Rev. A **58**, 2872 (1998); A. Kolakowska *et al.*, Phys. Rev. A **59**, 3588 (1999).

[11] M. Chassid and M. Horbatsch, Phys. Rev. A **66**, 012714 (2002).

[12] D. R. Schultz, C. O. Reinhold, P. S. Krstic, and M. R. Strayer, Phys. Rev. A. **65** 052722 (2002).

[13] R. Merzbacher R and H. W. Lewis, Hand. Phys. vol **34** (Berlin: Springer) pp 166-92 (1958).

[14] H. A. Bethe, L. Maximon, and F. Low , Phys. Rev. **91**, 417 (1953).

[15] J. Fu, Master's Thesis (Texas A&M University, 2000).

[16] M. Abramowitz and I. A. Stegun, *Handbook of Mathematical Functions* (Washington DC: National Bureau of Standards; Reprinted 1972 by New York: Dover Publications) (1964).

[17] A. Nordsieck, Phys. Rev. **93**, 785-787 (1954).

[18] I. S. Grandshiteyn and I. M. Ryzhik, *Table of Integrals, Series, and Products* (Academic Press, Inc., New York 1979).

[19] L. H. Thomas, Proc. Roy. Soc. A **114**, 561 (1927).

[20] M. H. Martir, Ph.D. Dissertation (Texas A&M University 1981).

[21] M. J. Fitzpatrick, Ph.D. Dissertation (Texas A&M University 2001).

[22] W. F. Smith, Ph.D. Dissertation (Texas A&M University 2001).

[23] L. H. Schick, Rev. Mod. Phys. **33**, 608 (1961).

[24] J. F. Reading and E. Fitchard, Phys. Rev. A **10**, 168 (1974).

[25] J. Binstock and J. F. Reading, Phys. Rev. A **11**, 1205 (1975).

[26] K. Ishii, K. Sera, A. Yamdera, M. Sebata, H. Arai and S. Morita, Phys. Rev. A **25**, 2511 (1982).

[27] J. F. Reading and J. Fu, Nuclear Instruments and Methods in Physics Research B **214**, 126 (2004).

# APPENDIX A

## SOME INTEGRALS INVOLVING BESSEL FUNCTION $J_L(KR)$

Note that $j_l(kr) = \left(\frac{\pi}{2kr}\right)^{1/2} J_{l+1/2}(kr)$. With the help of the following integral,

$$\begin{aligned}\int_0^\infty e^{-\alpha x} J_\nu(\beta x) x^\nu dx &= \frac{(2\beta)^\nu \Gamma\left(\nu+\frac{1}{2}\right)}{\sqrt{\pi}(\alpha^2+\beta^2)^{\nu+\frac{1}{2}}} \\ &\quad [\mathbf{Re}\nu > -\frac{1}{2}, \mathbf{Re}\alpha > |Im\beta|], \end{aligned} \tag{A.1}$$

we have

$$\begin{aligned}\int_0^\infty e^{-\alpha r} r^{l+1} j_l(kr) dr &= \int_0^\infty e^{-\alpha r} r^{l+1} \left(\frac{\pi}{2kr}\right)^{\frac{1}{2}} J_{l+1/2}(kr) dr \\ &= \left(\frac{\pi}{2k}\right)^{\frac{1}{2}} \frac{(2k)^{l+1/2}\Gamma(l+1)}{\sqrt{\pi}(\alpha^2+k^2)^{l+1}} \\ &= \frac{(2k)^l \Gamma(l+1)}{(\alpha^2+k^2)^{l+1}} \end{aligned} \tag{A.2}$$

Differentiate equation (A.2) with respect to $\alpha$ gives

$$\int_0^\infty e^{-\alpha r} r^{l+2} j_l(kr) dr = \frac{2\alpha(2k)^l \Gamma(l+2)}{(\alpha^2+k^2)^{l+2}} \tag{A.3}$$

$$\int_0^\infty e^{-\alpha r} r^{l+3} j_l(kr) dr = \frac{(2\alpha)^2(2k)^l \Gamma(l+3)}{(\alpha^2+k^2)^{l+3}} - \frac{2(2k)^l \Gamma(l+2)}{(\alpha^2+k^2)^{l+2}}. \tag{A.4}$$

# APPENDIX B

## ANOTHER METHOD TO EVALUATE INTEGRALS $I_2$ IN CHAPTER IV

To work out the exact expression of $\bar{V}\bar{z}_l(kr)$, use equation (4.16):

$$\bar{V}\bar{z}_l(kr) = \frac{1}{2}\frac{d^2}{dr^2}\bar{z}_l(kr) + \frac{1}{r}\frac{d}{dr}\bar{z}_l(kr) + \frac{1}{2}\left[k^2 - \frac{l(l-1)}{r^2}\right]\bar{z}_l(kr) \tag{B.1}$$

upon using the expression of $\bar{z}_l(kr)$ and the equation which $j_{l-1}$ satisfies, we have

$$\begin{aligned}\bar{V}\bar{z}_l(kr) &= \frac{1}{2}(1-e^{-\beta r})''j_{l-1}(kr) + (1-e^{-\beta r})'j'_{l-1}(kr) \\ &\quad + \frac{1}{r}(1-e^{-\beta r})'j_{l-1}(kr).\end{aligned} \tag{B.2}$$

From the following property of $j_l(\rho)$:

$$\frac{d}{d\rho}j_l(\rho) = j_{l-1}(\rho) - \frac{l(l+1)}{\rho}j_l(\rho) \tag{B.3}$$

$$j_{l-1}(\rho) + j_{l+1}(\rho) = \frac{2l+1}{\rho}j_l(\rho), \tag{B.4}$$

we have

$$\frac{d}{d\rho}j_l(\rho) = -j_{l+1}(\rho) - \frac{l^2-l-1}{\rho}j_l(\rho) \tag{B.5}$$

$$\frac{d}{d\rho}j_{l-1}(\rho) = -j_l(\rho) - \frac{l^2-3l+1}{\rho}j_{l-1}(\rho) \tag{B.6}$$

Thus we obtain

$$\begin{aligned}\bar{V}\bar{z}_l(kr) &= -\frac{\beta^2}{2}e^{-\beta r}j_{l-1}(kr) + \beta e^{-\beta r}(-k)\left[j_l(kr) + \frac{l^2-3l+1}{kr}j_{l-1}(kr)\right] \\ &\quad + \frac{\beta e^{-\beta r}}{r}j_{l-1}(kr).\end{aligned} \tag{B.7}$$

After simplification this gives

$$-\bar{V}\bar{z}_l(kr) = \frac{\beta^2}{2}e^{-\beta r}j_{l-1}(kr) + (l^2-3l)\frac{\beta e^{-\beta r}}{r}j_{l-1}(kr) + k\beta e^{-\beta r}j_l(kr). \tag{B.8}$$

The term in $I_2$ involving $l/r^2$ is

$$\begin{aligned} I_{22} &= \int_0^\infty r^2\chi_l(kr)\frac{l}{r^2}\bar{z}_l(kr)dr \\ &= l\cdot\sum a_i\int_0^\infty [e^{-\alpha_i r} - e^{-(\alpha_i+\beta)r}]r^l j_{l-1}(kr)dr \\ &= l\cdot\sum a_i\left[\text{BESINT}(\alpha_i,k,l-1,2) - \text{BESINT}(\alpha_i+\beta,k,l-1,2)\right]. \end{aligned} \tag{B.9}$$

The first term in $I_2$ involving $-\bar{V}$ is

$$\begin{aligned} I_{23} &= \int_0^\infty r^2\chi_l(kr)\frac{\beta^2}{2}e^{-\beta r}j_{l-1}(kr)dr \\ &= \frac{\beta^2}{2}\sum a_i\int_0^\infty e^{-\alpha_i r}r^{l+2}j_{l-1}(kr)dr \\ &= \frac{\beta^2}{2}\sum a_i\text{BESINT}(\alpha_i,k,l-1,3). \end{aligned} \tag{B.10}$$

The second term in $I_2$ involving $-\bar{V}$ is

$$\begin{aligned} I_{24} &= \int_0^\infty r^2\chi_l(kr)(l^2-3l)\beta\frac{e^{-\beta r}}{r}j_{l-1}(kr)dr \\ &= (l^2-3l)\beta\sum a_i\int_0^\infty e^{-(\alpha_i+\beta)r}r^{l+1}j_{l-1}(kr)dr \\ &= (l^2-3l)\beta\sum a_i\text{BESINT}(\alpha_i+\beta,k,l-1,2). \end{aligned} \tag{B.11}$$

The third term in $I_2$ involving $-\bar{V}$ is

$$\begin{aligned} I_{25} &= k\beta\int_0^\infty r^2\chi_l(kr)e^{-\beta r}j_l(kr)dr \\ &= k\beta\sum a_i\int_0^\infty e^{-(\alpha_i+\beta)r}r^{l+2}j_l(kr)dr \\ &= k\beta\sum a_i\text{BESINT}(\alpha_i+\beta,k,l,2). \end{aligned} \tag{B.12}$$

Since

$$I_2 = I_{21} + I_{22} + I_{23} + I_{24} + I_{25}, \tag{B.13}$$

to calculate $N_l$, use the following expression

$$N_l = \frac{1}{2k(I_{21} + I_{22} + I_{23} + I_{24} + I_{25} + iI_1)}. \tag{B.14}$$

Here $I_1$ is calculated as in Chapter IV.

# VITA

Jun Fu was born in 1973 in Shexian, Anhui Province, China, where he grew up and finished his high school. In August of 1991 he went to Nankai University in Tianjin, China. He received his B.S. degree in Physics in June 1995.

In August 1997 he came to Texas A&M University to pursue his graduate study. The following year he married Fengyu Song. In Dec. 2000 he received his master's degree in physics and began his Ph. D study in 2001. His research advisor was Dr. John F. Reading. The author can be reached through Dr. John F. Reading at the Physics Department, Texas A&M University, TX 77843-4242.

The typist for this dissertation was Jun Fu.